

Glass-like transition described by toppling of stability hierarchy

Jacek Grela* and Boris A Khoruzhenko†

*School of Mathematical Sciences, Queen Mary University of London,
Mile End Road, London E1 4NS, United Kingdom*

(Dated: June 3, 2021)

Building on the work of Fyodorov (2004) and Fyodorov and Nadal (2012) we examine the critical behaviour of population of saddles with fixed instability index k in high dimensional random energy landscapes. Such landscapes consist of a parabolic confining potential and a random part in $N \gg 1$ dimensions. When the relative strength m of the parabolic part is decreasing below a critical value m_c , the random energy landscapes exhibit a glass-like transition from a simple phase with very few critical points to a complex phase with the energy surface having exponentially many critical points. We obtain the annealed probability distribution of the instability index k by working out the mean size of the population of saddles with index k relative to the mean size of the entire population of critical points and observe toppling of stability hierarchy which accompanies the underlying glass-like transition. In the transition region $m = m_c + \delta N^{-1/2}$ the typical instability index scales as $k = \kappa N^{1/4}$ and the toppling mechanism affects whole instability index distribution, in particular the most probable value of κ changes from $\kappa = 0$ in the simple phase ($\delta > 0$) to a non-zero value $\kappa_{\max} \propto (-\delta)^{3/2}$ in the complex phase ($\delta < 0$). We also show that a similar phenomenon is observed in random landscapes with an additional fixed energy constraint and in the p -spin spherical model.

* jacekgrela@gmail.com

† b.khoruzhenko@qmul.ac.uk

I. INTRODUCTION

Low-dimensional random fields for a long time held a prominent role in sciences as many natural phenomena are described through statistics of random fields defined on either space or space-time [11] with typical dimensionalities $N = 2, 3$ or 4 . On the other hand, only recently high-dimensional spaces ($N \gg 1$) received attention with the advent of machine learning [20] or in studies of complex systems like spin glasses and large bio-molecules [30]. In such applications, the dimensionality N is identified with the number of degrees of freedom and the field itself is interpreted as either energy function (spin glasses, proteins) or loss function (machine learning). As was pointed out and utilized numerous times [5, 10, 25], the task is always to find a configuration of the system such that the energy (or loss) function is minimized.

Although this task is straightforward in low dimensions, its successful completion for non-convex surfaces in high-dimensional spaces is notoriously intractable and is a NP-hard problem. As a result, *heuristic* methods, e.g., algorithms which work approximately but whose robustness remain elusive, are widespread and remain the main choice of tool for practitioners. A well-known example is the stochastic gradient descent (SGD) algorithm derived from a gradient descent method for solving convex problems.

Almost all problems with minimizing non-convex functions are ultimately related to the structure of their surface which varies just as the Earth's landscape does with plateaus, valleys and peaks only with a greater degree of variability. On top of that, the landscape described is very high-dimensional and thus heavily impeding our intuition. Despite these difficulties, insights into behaviour of energy/loss landscapes are crucial in understanding of the success of algorithms like SGD. In this context, the most natural approach is to study quantities related to stationary points of the function by either counting their total number or study their respective positions.

In recent years, perhaps the most glaring case of a successful approach to non-convex optimization is that of Deep Neural Networks (DNNs). Not only the success of training DNNs through SGD is surprising, also such models do not suffer from *overfitting* despite being extremely overparametrized, generalize well to unseen examples and do not get stuck in local minima [24]. One possible explanation of these features [10] is provided by inspecting statistics of stationary points of the DNN loss function based on an explicit link to spherical spin glass models. This approach along with related works [2, 3] offers a possible explanation of trainability aspects of DNNs through analyzing structure of stationary points. Our work extends this line of inquiry through a probabilistic approach to the description of populations of stationary points having a fixed instability index.

The aim of our work is to offer a detailed analysis of the stationary points in the energy landscapes of systems undergoing glass-like transition. The existing body of work on this subject mostly focuses on parameter ranges far from the critical threshold, both in the topologically non-trivial phase (where stationary points are exponentially abundant) and in the topologically trivial phase (where, typically, there are very few stationary points) [9, 16, 17, 19]. To the best of our knowledge, the only work providing insights into what happens near the critical threshold is one by Fyodorov and Nadal [18] who counted minima. We complement this study by tracking the relative sizes of populations of minima, maxima as well as saddle points with any given instability index k (number of unstable directions) *near the critical threshold*. To this end, we work out fractional probabilities p_k for a stationary point to have a given instability index k , an approach introduced in [7]. These probabilities are quotients of the population size of the stationary points with index k to the total number of the stationary points. The picture which is emerging from our analysis offers an alternative explanation of the glass-like transition based on *toppling of stability hierarchy* of populations of stationary points. In this context, the stability hierarchy refers to a steady decrease of p_k when the instability index k is increasing, so that local minima are the most likely stationary points, while toppling refers to a sudden change when the most likely stationary points are those with a fixed number of unstable directions $k_{max} > 0$. As we show in the current work, this phenomenon which marks a global change in the underlying random landscape is shared by a number of models.

Acknowledgements. We thank F. Bornemann for sharing with us the package *RMTFredholmToolbox* [8] used to calculate Tracy-Widom distributions.

II. MAIN RESULTS

In order to gain insights into statistics of stationary points in the transition region, we employ the paradigmatic model [15, 17] of random energy landscape where a random scalar field is coupled to a parabolic confining potential with the transition driven by the coupling strength $\mu > 0$:

$$E(\mathbf{x}) = \frac{\mu}{2} |\mathbf{x}|^2 + V(\mathbf{x}). \quad (1)$$

Here \mathbf{x} is a vector in N -dimensional state-space and $V(\mathbf{x})$ is isotropic homogeneous Gaussian vector field with zero mean value and covariance function

$$\langle V(\mathbf{x})V(\mathbf{x}') \rangle = Nf\left(\frac{|\mathbf{x} - \mathbf{x}'|^2}{2N}\right). \quad (2)$$

The main feature of model (1) is the existence of two distinct phases in the thermodynamic limit $N \rightarrow \infty$ with a sharp transition region between the two phases at $\mu_c = \sqrt{f''(0)}$ [17]. Introducing the rescaled coupling strength $m = \mu/\mu_c$, $m_c = 1$, for large values of m the system is in a topologically trivial phase whereby the parabolic confining potential dominates the energy landscape (the probability of finding more than one stationary point is zero in the limit $N \rightarrow \infty$). As m decreases below the critical threshold at $m = 1$ the energy landscape becomes highly complex which manifests itself in an exponential explosion of stationary points - the (average) total number of stationary points and the number of local minima grow exponentially as the dimension of the state space N increases. This transition is frequently called glass-like as it is closely related to one found in spherical spin-glasses [6].

In a natural way, the energy landscape (1) gives rise to a gradient flow which is defined by the differential equation

$$\dot{\mathbf{x}} = -\nabla E(\mathbf{x}). \quad (3)$$

Then the stationary points \mathbf{x}_* of $E(\mathbf{x})$, i.e., the points where ∇E vanishes, are the equilibria (fixed points) of the gradient flow (3). In this picture, if \mathbf{x}_* is a point of local minimum of $E(\mathbf{x})$ (i.e., all eigenvalues of the Hessian $(\partial_i \partial_j E(\mathbf{x}))_{ij}$ at $\mathbf{x} = \mathbf{x}_*$ are positive) then the equilibrium \mathbf{x}_* is asymptotically stable. That is, a small displacement from \mathbf{x}_* in any direction results in the system asymptotically returning back to \mathbf{x}_* . If \mathbf{x}_* is a saddle and k is the number of negative eigenvalues of the Hessian of $E(\mathbf{x})$ at $\mathbf{x} = \mathbf{x}_*$ then the equilibrium at \mathbf{x}_* will have $N - k$ stable directions displacements along which will result in the system asymptotically returning back. In this way, the index k is a measure of instability of equilibrium at $\mathbf{x} = \mathbf{x}_*$. The higher the value of k is, the fewer stable directions there will be at the equilibrium. Obviously, local maxima, i.e., stationary points where $k = N$, are most unstable. We shall call k the instability index.

A. Populations of stationary points

In this work, we go beyond counting few sub-populations (like minima) of stationary points in absolute terms and instead work out relative or fractional probability distributions for finding stationary points with fixed instability index. This approach enables novel, refined questions like:

- Given a randomly sampled stationary point, what would be its most likely instability index? How does a full probability distribution of indices look like?
- How does the probability distribution of indices change in the vicinity of transition region?

Such pertinent enquiries can be made by a local agent (like an SGD algorithm or glassy system looking for a configuration minimizing its energy) probing the landscape and encountering saddles on its way. For example, it was argued in ref. [23] that the abundance of saddles with a large number of stable directions leads to slowing down the gradient descent dynamics in high dimensional energy landscapes due to the dominance of borders in high dimensions: at low temperatures the system is trapped for long times near borders (ridges) of basins of attraction of local minima and the gradient descent is determined mainly by nearby saddles.

In what follows, we utilize three interrelated counting statistics:

- \mathcal{N}_k , the number of stationary points with instability index k ;
- $\mathcal{N}_{\text{eq}} = \sum_{k=0}^N \mathcal{N}_k$, the total number of stationary points;
- $\mathcal{N}^{(k)} = \sum_{n=0}^k \mathcal{N}_n$ the number of stationary points with instability index up to k .

The quotient of the first two counting statistics is the relative frequency $\mathcal{N}_k/\mathcal{N}_{\text{eq}}$ of saddles with instability index k , whilst the last one is the associated cumulative frequency distribution $\mathcal{N}^{(k)}/\mathcal{N}_{\text{eq}}$. If \mathbf{x}_* is a stationary point of $E(\mathbf{x})$ drawn at random from the entire population of stationary points then, as was shown in [7], the probability for \mathbf{x}_* to have k unstable directions is given by the average of $\mathcal{N}_k/\mathcal{N}_{\text{eq}}$ over the realizations of the random field $V(\mathbf{x})$:

$$\text{Pr}\{\mathbf{x}_* \text{ has instability index } k\} = \langle \mathcal{N}_k/\mathcal{N}_{\text{eq}} \rangle. \quad (4)$$

Therefore, $\langle \mathcal{N}_k / \mathcal{N}_{\text{eq}} \rangle$ and $\langle \mathcal{N}^{(k)} / \mathcal{N}_{\text{eq}} \rangle$ are, respectively, the probability density function (pdf) and cumulative distribution function (cdf) of the instability index k .

In the context of the above two questions, calculating both averages is a natural starting point. This seems a prohibitively difficult task, and, instead, we set out to analyse the *annealed* probabilities

$$p_k = \frac{\langle \mathcal{N}_k \rangle}{\langle \mathcal{N}_{\text{eq}} \rangle}, \quad P_k = \frac{\langle \mathcal{N}^{(k)} \rangle}{\langle \mathcal{N}_{\text{eq}} \rangle}. \quad (5)$$

where enumerator and denominator are averaged separately and combined afterwards. To justify a connection between the right-hand side in Eq. (4) and its annealed counterpart p_k , counting statistics in both enumerator and denominator ought to have a self-averaging property in the limit of high dimensionality $N \rightarrow \infty$ limit. The recent works [27] and [4] addressed this question for the pure p -spin spherical model whose energy landscape falls in the same class as the random energy model and gave an affirmative answer for equilibria with finite instability index k . This gives rise to a hope that for some classes of coupling fields the annealed picture will resemble the quenched one. The task of identifying such classes of coupling fields is a challenging open problem which deserves further investigations.

The picture that is emerging from our analysis is described below.

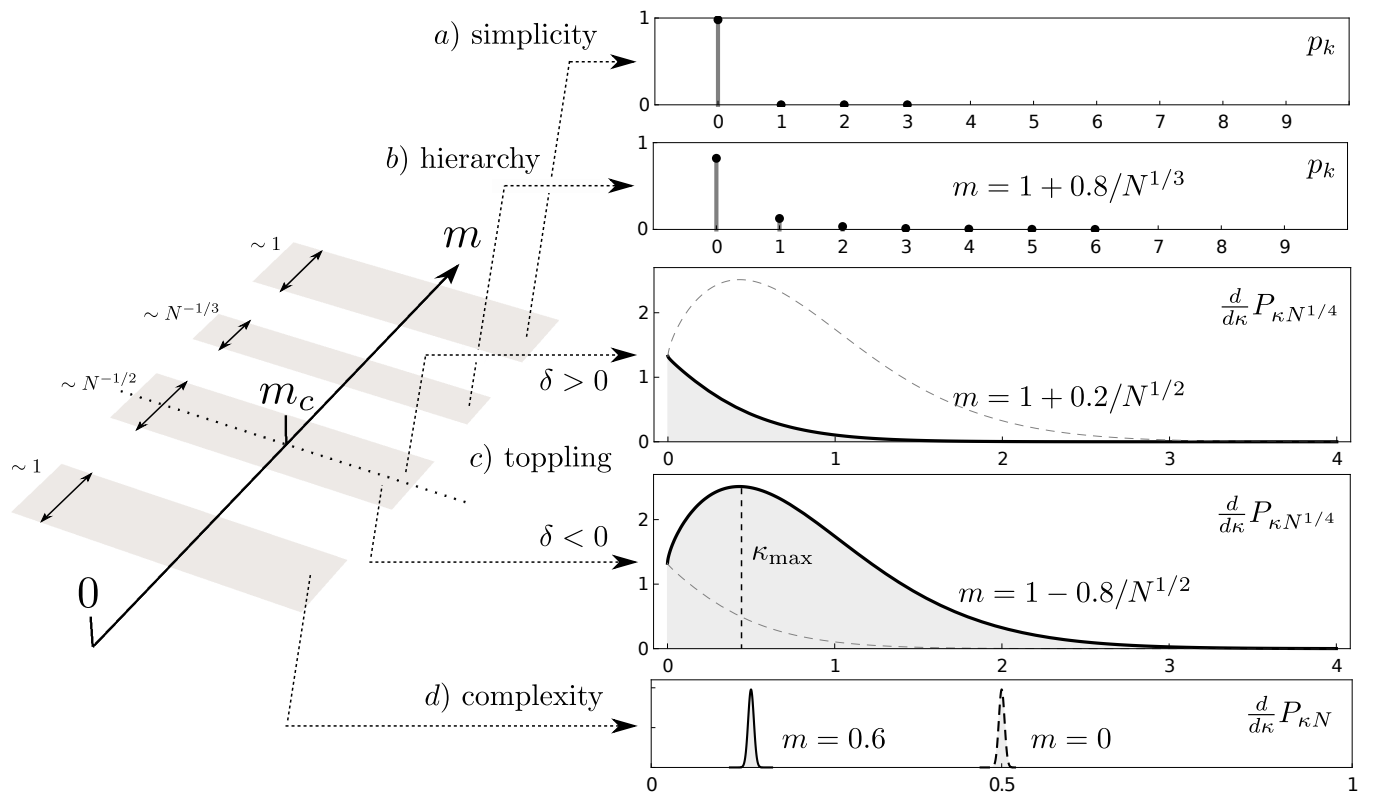


Figure 1. Diagram illustrating toppling mechanism in the random energy landscape model in the limit of high dimensionality $N \gg 1$. Five plots on the right-hand side show density of the annealed distribution of the instability index k in each of the four scaling regions, see Tab. I for analytic expressions. The two plots in the simplicity and hierarchy regions are discrete as the instability index k takes finite integer values there, while the two plots in the toppling region and the plot in the complexity region are continuous as the instability index scales in these regimes with $N^{1/4}$ and N respectively. In plot c) $\kappa_{\text{max}} = \frac{4\sqrt{2}}{3\pi}(-\delta)^{3/2}$ when $\delta < 0$. Plot b) was evaluated using numerical package [8].

B. Toppling of stability hierarchy

As was mentioned above, one manifestation of the phase transition in the random energy model (1)–(2) is the exponential explosion in the number of stationary points. In the limit of high dimensionality $N \rightarrow \infty$, the complexity

exponents

$$\Sigma_{\text{eq}} = \lim_{N \rightarrow \infty} \frac{1}{N} \ln \langle \mathcal{N}_{\text{eq}} \rangle \quad \text{and} \quad \Sigma_0 = \lim_{N \rightarrow \infty} \frac{1}{N} \log \langle \mathcal{N}_0 \rangle \quad (6)$$

associated, respectively, with the total number of stationary points and the number of local minima, are positive for every $m < 1$,

$$\Sigma_{\text{eq}} = \frac{m^2 - 1}{2} - \ln m, \quad \Sigma_0 = \Sigma_{\text{eq}} - (1 - m)^2, \quad (0 < m < 1) \quad (7)$$

and zero for every $m > 1$ [17, 18]. However, as can be seen from Eq. (7) these two counting statistics develop the exponential growth on different scales at the critical threshold: the width of the transition region for $\langle \mathcal{N}_{\text{eq}} \rangle$ is $N^{-1/2}$, whilst the width of the transition region for $\langle \mathcal{N}_0 \rangle$ is $N^{-1/3}$. When one analyzes the relative sizes of populations of stationary points near the critical threshold, such as the annealed probabilities p_k and P_k of Eq. (5), the microscopic scales get superimposed. This suggests that the glassy transition in model (1)–(2) has several distinct transition regions which we will now describe.

It is convenient to encode the scaling regimes by the formula

$$m = 1 + \frac{\delta}{N^\beta}.$$

The parameter values $\beta = 1/2$ and $\beta = 1/3$ define the two aforementioned microscopic scales and the parameter value $\beta = 0$ defines a global scale. Based on these three natural scales, we can identify four distinct scaling regions of change consisting of two microscopic and two macroscopic scales, see Fig. 1 and Tab. I:

a) *Simplicity region*, $m = 1 + \delta > 0$

In this region the parabolic confining potential dominates in the limit $N \rightarrow \infty$. The instability index k is a discrete variable and $k = 0$ corresponds to a minima. With probability asymptotically close to 1 the system has only one stationary point which is a local minimum, and so $p_k \sim 1$ in the limit $N \rightarrow \infty$ if $k = 0$ and $p_k \sim 0$ otherwise. This is illustrated in plot a), Fig. 1.

b) *Hierarchy region*, $m = 1 + \delta/N^{1/3}$, $\delta > 0$

As the value of m is decreasing and getting closer to the critical threshold $m_c = 1$, the system exits the simplicity region and enters a hierarchy region. In this region the mean number of saddles $\langle \mathcal{N}_{\text{eq}} \rangle$ is increasing as m gets closer to 1 (but staying finite in the limit of high dimensionality) and the deviations of the instability index k from zero become larger. This results in a flow of indices away from $k = 0$ and the emergence of groups of increasingly more unstable saddles as evidenced by non-zero values of $\langle \mathcal{N}_k \rangle$ for $k > 0$, see Tab. I. Consequently, the annealed probability distribution of the instability index k develops a non-zero tail extending to finite values of k and displaying the hierarchy of stability $p_0 > p_1 > p_2 > \dots$ with the most likely stationary point being a local minimum. This is illustrated in plot b), Fig. 1. Note that typical values of the instability index k do not scale with N in the limit of high dimensionality, i.e. k takes finite values $k = 0, 1, 2, \dots$

c) *Toppling region*, $m = 1 + \delta/N^{1/2}$, $\delta \in \mathbb{R}$

As the value of m is decreasing further and getting closer to the critical threshold, the flow of indices away from zero becomes stronger and their distribution flatter, i.e., the difference between p_k and p_{k+1} is becoming smaller and smaller. This microscopic mechanism is fundamental and eventually leads to a macroscopic change which occurs in the region $m = 1 + \delta/N^{1/2}$. It can be shown that in this region the total number of stationary points scales as $N^{1/4}$ and so do typical values of the instability index k . It is then natural to introduce rescaled instability index $\kappa = k/N^{1/4}$ which becomes a continuous random variable in the limit of high dimensionality. It is instructive to inspect the dependence of the rescaled index density $\frac{d}{d\kappa} P_{\kappa N^{1/4}}$ on parameter δ , see Fig. 1 and Tab. I. For every fixed $\delta > 0$, this density is monotonically decreasing function of κ in the interval $0 \leq \kappa < \infty$ and, hence, the hierarchy developed in region b) persists. The transition point ($\delta = 0$) is the tipping point. For every fixed $\delta < 0$, the index density is a unimodal function of κ attaining its maximum value at $\kappa_{\text{max}} = \frac{4\sqrt{2}}{3\pi} (-\delta)^{3/2}$. The loss of monotonicity means that the most likely stationary point is no longer a local minimum but instead a saddle with $\kappa_{\text{max}} N^{1/4}$ unstable directions. In other words, the hierarchy of stationary point populations is broken and transition to complex phase starts which eventually produces a typical (i.e. most probable) stationary point with non-zero instability index.

d) *Complexity region*, $0 < m < 1$

As the scaled coupling strength m is decreasing further below the critical threshold, the system enters the topologically non-trivial phase where the total number of stationary points is exponential in N , see Eq. (7). In this region, typical values of k as N and thus $\kappa = k/N \in (0, 1)$ can be interpreted as finite fraction of all possible saddles. The resulting index density $\frac{d}{d\kappa} P_{\kappa N}$ has a highly localized peak at

$$\begin{aligned} \kappa_{max}(m) &= \int_m^1 \rho_{sc}(\lambda) d\lambda, & \rho_{sc}(\lambda) &= \frac{2}{\pi} \sqrt{1 - \lambda^2} \\ &= \frac{1}{\pi} \left(\arccos m - m\sqrt{1 - m^2} \right) \end{aligned}$$

see plot d), Fig. 1. As one would expect $\kappa_{max}(1) = 0$ and $\kappa_{max}(0) = 1/2$, so that when the parabolic confining potential is turned off completely, the most likely instability index is $N/2$ as for a pure random field stable and unstable directions are equally likely.

All formulas described above are written down explicitly and summarized in Tab. I while all the derivations are found in Sec. III.

Table I. Annealed cumulative distribution $P_k = \langle \mathcal{N}^{(k)} \rangle / \langle \mathcal{N}_{eq} \rangle$ of the instability index k in the random energy landscape model (1)–(2) in the limit of high dimensionality $N \gg 1$. Here, $\rho_{edge}(\lambda) = (\text{Ai}'(\lambda))^2 - \lambda(\text{Ai}(\lambda))^2 + \frac{1}{2}\text{Ai}(\lambda) \left(1 - \int_{\lambda}^{\infty} \text{Ai}(t) dt\right)$ and $\rho_{sc}(\lambda) = \frac{2}{\pi} \sqrt{1 - \lambda^2}$ are the eigenvalue densities at the edge and in the bulk of the eigenvalue distribution in the GOE, and $F_n(\lambda)$ is the cdf of the top $(n + 1)$ -st eigenvalue in the GOE. The complexity exponent Σ_{eq} is given in Eq. 7 and $c = (3\pi/(4\sqrt{2}))^{2/3}$. Distribution densities in the third column are plotted in Fig. 1

Coupling strength m	Cumulative distribution P_k	Density of distribution	Total number of saddles $\langle \mathcal{N}_{eq} \rangle$
$m = 1 + \delta, \quad \delta > 0$	$\sum_{n=0}^k p_n$	$p_n = \delta_{n,0}$	1
$m = 1 + \frac{\delta}{\sqrt[3]{N}}, \quad \delta > 0$	$\sum_{n=0}^k p_n$	$p_n = \frac{\int_{-\infty}^{\infty} e^{\delta\lambda} dF_n(\lambda)}{\int_{-\infty}^{\infty} e^{\delta\lambda} \rho_{edge}(\lambda) d\lambda}$	$2e^{-\frac{\delta^3}{3}} \int_{-\infty}^{\infty} e^{\delta\lambda} \rho_{edge}(\lambda) d\lambda$
$m = 1 + \frac{\delta}{\sqrt{N}}, \quad \delta \in \mathbb{R}$	$\int_0^{\frac{k}{\sqrt{N}}} p(x) dx$	$p(x) = c \frac{e^{-(\delta+cx^{2/3})^2}}{\int_0^{+\infty} e^{-(\delta+cx^{2/3})^2} dx}$	$2N^{1/4} e^{\delta^2} \int_0^{+\infty} e^{-(\delta+cx^{2/3})^2} dx$
$m = 1 - \delta, \quad \delta \in (0, 1)$	$\int_0^{k/N} p(x) dx$	$p(x) = \delta \left(x - \int_m^1 \rho_{sc}(\lambda) d\lambda \right)$	$\sqrt{4\pi N} \rho_{sc}(m) e^{N\Sigma_{eq}(m)}$

C. Universality of the toppling mechanism

Although in this work we explain glass-like transition through toppling of stability hierarchy on the toy model (1), we believe it holds more generally. To support this claim, in Apps. B and C we report on analogous mechanisms driving the transition in the model (1) with an additional fixed energy constraint [19] and in the spherical spin-glass model [3, 12, 16, 22].

Firstly, in the fixed energy model we consider an energy function (1) with additional constraint $E_0 = E(\mathbf{x})$ thus extending its phase space to two dimensions with the coupling strength m defined previously and rescaled energy value $\epsilon_0 \sim E_0/N$. The left plot in Fig. 2 depicts full macroscopic phase space of the constrained model while the right plot focuses solely on the region around the critical gray square at $m = 1, \epsilon_0 = -\frac{1}{2q}$ (q is a fixed parameter set by random field correlation function and its derivatives all evaluated at zero). In what follows we focus only on the toppling region which is a rectangular area of size $O(N^{-1/2})$ around this critical point. In the right plot of Fig. 2 we see in detail how minor modification of the model (1) alters the vicinity of the glass-like transition. Although for $\delta > 0$ the only meaningful path (where $\Sigma_{eq} \geq 0$ so that fractional probabilities (5) make sense) goes along line $\epsilon = 0$, for $\delta < 0$ all energy parameters $\epsilon \in (\epsilon_+, \epsilon_-)$ with $\epsilon_{\pm} = \delta \left(-\frac{3}{2q} \pm \frac{\sqrt{3+2q^2}}{q} \right)$ comprise valid paths (crossed out region in Fig. 2). From a macroscopic point of view, a one-dimensional hierarchy region for $m > 1$ transitions to

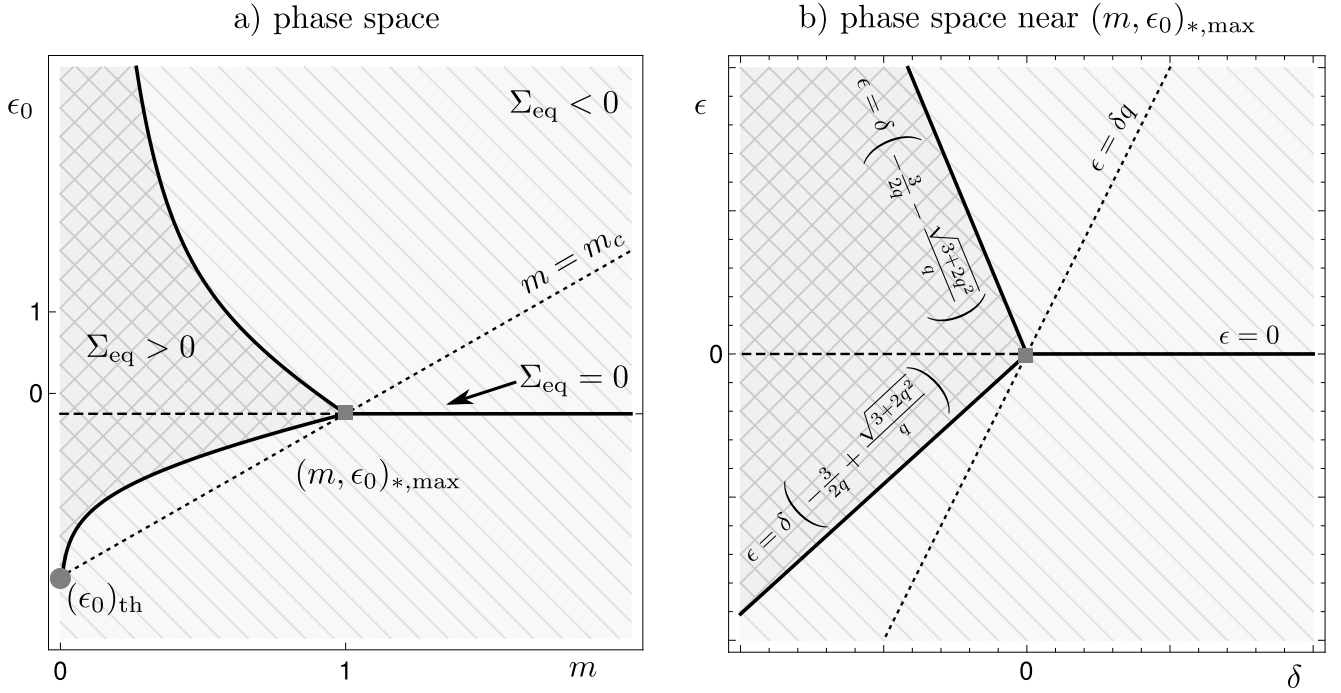


Figure 2. Phase space in the fixed energy model (B1) in a) macroscopic variables (m, ϵ_0) variables and b) microscopic $(m, \epsilon_0) = (m, \epsilon_0)_{*,\max} + (\delta, \epsilon)N^{-1/2}$ near critical point $(m, \epsilon_0)_{*,\max} = (1, -1/(2q))$. All notation is defined in App. B. (Left plot) Macroscopic phase space. Slanted dotted line is the $m = m_c$ boundary where both complexity functions found in Eqs. (B7) and (B8) coincide $\Sigma_{\text{eq}}^>(m = m_c) = \Sigma_{\text{eq}}^<(m = m_c)$. Crossed out region is where complexity function is positive $\Sigma_{\text{eq}} > 0$ while dashed region is where $\Sigma_{\text{eq}} < 0$. Thick black lines in both $m > m_c$ and $m < m_c$ are the critical boundaries when the complexity function vanishes $\Sigma_{\text{eq}} = 0$. Thin dashed line denotes the critical value $\epsilon_0 = -\frac{1}{2q}$. Gray square marks the critical value $(m, \epsilon_0)_{*,\max}$ while a gray dot denotes the threshold energy value $(\epsilon_0)_{\text{th}} = -\frac{1+2q^2}{2q}$. (Right plot) Microscopic phase space expanded around critical point $(m, \epsilon_0)_{*,\max}$. All colors and line styles are consistent with the left plot.

a two-dimensional complexity region for $m < 1$ after passing through the transition point at $m = 1$. The discussed transition is connected with the toppling mechanism as manifested in the form of annealed cumulative distribution:

$$P_k(\delta, \epsilon) \sim \frac{\int_0^{\frac{k}{\sqrt[3]{N}}} e^{-(\Delta_q(\delta, \epsilon) + c_q x^{2/3})^2} dx}{\int_0^{+\infty} e^{-(\Delta_q(\delta, \epsilon) + c_q x^{2/3})^2} dx} \quad (8)$$

where

$$c_q = \sqrt{\frac{2q^2 + 3}{2q^2 - 1}} \left(\frac{3\pi}{4\sqrt{2}} \right)^{2/3}, \quad \Delta_q(\delta, \epsilon) = \frac{2\sqrt{2}q^2}{\sqrt{(2q^2 - 1)(q^2 + 2)}} \left(\delta - \frac{\epsilon}{q} \right). \quad (9)$$

For fixed q , c_q is a constant and $\Delta \propto \delta - \epsilon/q$. The behaviour of function (8) is driven by the sign of $\Delta_q(\delta, \epsilon)$ so the condition $\Delta_q(\delta, \epsilon) = 0$ describes a boundary line along which toppling takes place (see dotted line in right plot of Fig. 2). When we take into account only meaningful paths when the complexity function of total number of stationary points is non-negative $\Sigma_{\text{eq}} \geq 0$, we recreate the toppling mechanism in two-dimensional phase space. In particular, system develops the most probable non-zero instability index $\kappa'_{\max} = \left(-\frac{\Delta_q(\delta, \epsilon)}{2c_q} \right)^{3/2}$ during the transition while the main features of probability plots mirror that of the unconstrained model presented in Fig. 1. Furthermore, connection with the unconstrained model is evident as the fractional probabilities in the toppling region in this model have the same functional form as Eq. (8) (see Tab. I).

Secondly, the spherical spin-glass model is defined by an energy function

$$E_o(\mathbf{x}) = \sum_{i_1, \dots, i_p=1}^{N+1} J_{i_1, i_2, \dots, i_p} x_{i_1} x_{i_2} \dots x_{i_p} + \sum_{i=1}^{N+1} h_i x_i, \quad (10)$$

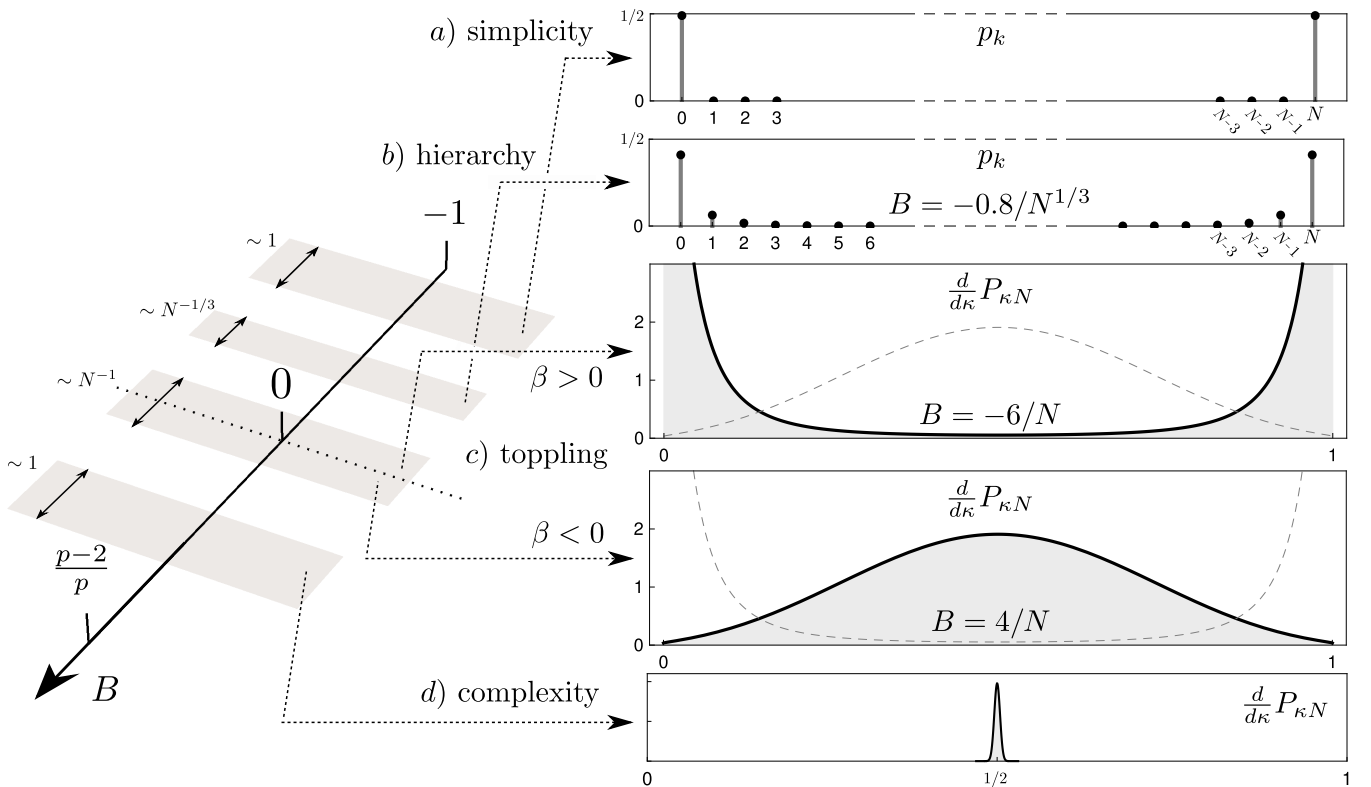


Figure 3. Diagram illustrating toppling mechanism in the spherical spin-glass model in the limit of high dimensionality $N \gg 1$. Five plots on the right-hand side show density of the annealed distribution of the instability index k in each of the four scaling regions, see Tab. II for analytic expressions. The two plots in the simplicity and hierarchy regions are discrete as the instability index k takes finite integer values there, while the two plots in the toppling region and the plot in the complexity region are continuous as the instability index scales in these regimes with N . Plot b) was evaluated using numerical package [8].

where \mathbf{x} is an $N + 1$ dimensional vector constrained to lie on the sphere $\sum_{i=1}^{N+1} x_i^2 = N$ and $p \geq 2$ is a positive integer. Symmetric coupling matrix J and random external field h_i are both drawn from Gaussian distributions with vanishing means and variances

$$\langle (J_{i_1 i_2 \dots i_p})^2 \rangle = \frac{J^2}{pN^{p-1}}, \quad \langle h_i^2 \rangle = \sigma^2. \quad (11)$$

In App. C we both recall known results and summarize new calculations enabling calculation of asymptotic forms of annealed probabilities across regions a)-d), see Tab. II for a summary. In Fig. 3 we plot these probabilities in all four regions as a function of an effective variable $B = \frac{J^2(p-2) - \sigma^2}{J^2 p + \sigma^2}$ combining variances J, σ and parameter p . Importantly, although at first the resulting picture might not resemble Fig. 1 plotted for the toy model (1), it is due to development of a dual hierarchy resulting in likewise toppling of both hierarchies simultaneously.

In contrast to the toppling mechanism of model (1) where around a single minimum in the simple region one hierarchy is developed, in the spherical model, by topological reasons, the simple phase consists instead of two stationary points – a minimum and a maximum. These in turn produce two disjoint stability hierarchies and eventually, in the toppling region both hierarchies are toppled as they merged together to create a joint density centered around scaled instability index $\kappa = 1/2$. Complexity region is trivial and centered around $\kappa = 1/2$ so the toppling mechanism happens on a smaller scale.

D. Conclusions

In this work we propose a detailed picture of glass-like transition described through the lens of stationary point populations. To this end, we work out fractional probabilities of populations of stationary points with fixed number of unstable directions. Their behaviour changes as the system changes between simple and complex phases where

Table II. Annealed distribution $P_k = \langle \mathcal{N}^{(k)} \rangle / \langle \mathcal{N}_{\text{eq}} \rangle$ of the instability index k in the spherical spin-glass model (10)–(11) in the limit of high dimensionality $N \gg 1$. The first two scaling regimes are expanded for two different parameter ranges of k due to topological constraint linking stability and instability in the spherical model. $\rho_{\text{edge}}(\lambda)$, $\rho_{\text{sc}}(\lambda)$ and $F_n(\lambda)$ are as defined in Tab. I and Q_x is the quantile function of the semicircular law, $\int_{Q_x}^1 \rho_{\text{sc}}(\lambda) d\lambda = x$. The mean total number of saddles $\langle \mathcal{N}_{\text{eq}} \rangle$ in all four regimes was obtained in ref. [16].

$B = \frac{J^2(p-2) - \sigma^2}{J^2 p + \sigma^2}$	Cumulative distribution P_k	Density of distribution	Total number of saddles $\langle \mathcal{N}_{\text{eq}} \rangle$
$-1 < B < 0$	$P_k = \sum_{n=0}^k p_n, P_{N-k} = 1 - P_k$	$p_n = \frac{1}{2} \delta_{n,0}, p_{N-n} = p_n$	2
$B = -\frac{\delta}{\sqrt[3]{N}}, \delta > 0$	$P_k = \sum_{n=0}^k p_n, P_{N-k} = 1 - P_k$	$p_n = \frac{1}{2} \frac{\int_{-\infty}^{\infty} e^{\delta\lambda} dF_n(\lambda)}{\int_{-\infty}^{\infty} e^{\delta\lambda} \rho_{\text{edge}}(\lambda) d\lambda}, p_{N-n} = p_n$	$4e^{-\frac{\delta^3}{3}} \int_{-\infty}^{\infty} e^{\delta\lambda} \rho_{\text{edge}}(\lambda) d\lambda$
$B = -\frac{\delta}{N}, \delta \in \mathbb{R}$	$\int_0^{k/N} p(x) dx$	$p(x) = \frac{e^{\delta Q_x^2}}{\int_{-1}^1 e^{\delta\lambda^2} \rho_{\text{sc}}(\lambda) d\lambda}$	$2Ne^{-\delta} \int_{-1}^1 e^{\delta\lambda^2} \rho_{\text{sc}}(\lambda) d\lambda$
$0 < B \leq \frac{p-2}{p}$	$\int_0^{k/N} p(x) dx$	$p(x) = \delta\left(x - \frac{1}{2}\right)$	$4\sqrt{N} \sqrt{\frac{1+B}{\pi B}} e^{\frac{N}{2} \log \frac{1+B}{1-B}}$

its energy landscape contains few and many stationary points respectively. In the simple phase, the system develops a hierarchy of stability defined as monotonic behaviour of fractional probabilities – most probable stationary points are minima (with instability index $k = 0$), then stationary points with $k = 1$ are less probable and so on. Such an ordering of populations of stability points is first developed and then broken down as the system passes towards the complex phase which we refer to as the *toppling of stability hierarchy*. In the vicinity of the transition, we identify the toppling as breaking of the monotonicity of fractional probabilities of populations or as change in hierarchy where minima cease to be the most probable population of stationary points.

Although our analysis is based mainly on one toy model, we argue that discussed mechanism is a universal feature of glass-like transition. To this end, we work out a model (1) with fixed energy constraint modifying the vicinity of the glassy transition and the spherical spin-glass model (10) introducing a toppling of dual hierarchy. In both cases the toppling of stability hierarchy explained the transition which we believe is a general feature as the models become linked to properties of the underlying random matrix which in turn have known universal properties [1]. We strengthen that point by presenting all final formulas for counting functions in a single notation depending ultimately on probability densities of ordered eigenvalues of random matrices.

III. CALCULATIONS

In this part we provide readers with detailed derivations of results discussed in Sec. II. Fractional probabilities (5) are composed of three quantities – $\langle \mathcal{N}_{\text{eq}} \rangle$, mean number of all stationary points, mean number of points with instability index k given by $\langle \mathcal{N}_k \rangle$ and mean number of points with instability index up to k given by $\langle \mathcal{N}^{(k)} \rangle$. We calculate exact and asymptotic expressions compiling together both known and new results.

Firstly, the main formula is derived in Sec. III A for the number of stationary points with fixed instability index k :

$$\langle \mathcal{N}_k \rangle = c_N m^{-N} \sqrt{N} \int_{-\infty}^{\infty} ds e^{-Nf(s;m)} \rho_{N+1}^{(k+1)}(\sqrt{N}s), \quad (12)$$

with constant $c_N = \sqrt{\frac{2}{\pi}} \left(\frac{2}{N}\right)^{N/2} \Gamma\left(\frac{N+1}{2}\right)$, function $f(s;m) = \left(s - \frac{m}{\sqrt{2}}\right)^2 - \frac{s^2}{2}$ and $\rho_N^{(k)}$ being the density of k -th largest eigenvalue of random $(N+1) \times (N+1)$ sized matrix drawn from a Gaussian Orthogonal Ensemble (GOE). To authors knowledge, Eq. (12) was not explicitly written out in the literature apart from the case $k = 0$ considered in [18] and the same quantity computed in the spherical model [3]. Formula for the cumulative number $\langle \mathcal{N}^{(k)} \rangle = \sum_{n=0}^k \langle \mathcal{N}_n \rangle$

is a sum of $k + 1$ contributions (12) while for $k = N$, the cumulative mean number reduces to the total number of stationary points since $\langle \mathcal{N}^{(N)} \rangle = \langle \mathcal{N}_{\text{eq}} \rangle$.

In the next Section we the asymptotic forms of Eq. (12) and its cumulative counterpart in the four regions across the transition point. For completeness, in Sec. III C we obtain the expression for the mean number of all stationary points $\langle \mathcal{N}_{\text{eq}} \rangle$ [17] from Eq. (12) and in Sec. III D we obtain the mean $\langle \mathcal{N}_{\text{eq}} \rangle$ in the four regions across the transition point recovering results of [16].

A. Calculating $\langle \mathcal{N}_k \rangle$ or the mean number of stationary points with index k

Counting statistics for populations of stationary points are given in terms of formal density

$$\rho_k(\mathbf{x}) = \sum_{\mathbf{x}_*^{(k)}} \delta(\mathbf{x} - \mathbf{x}_*^{(k)}), \quad (13)$$

where the summation is over all stationary points $\mathbf{x}_*^{(k)}$ with fixed instability index k . This density is in turn expressed by the celebrated Kac-Rice formula

$$\rho_k(\mathbf{x}) = |\det \partial_{ij} E(\mathbf{x})| \Theta_k(\partial_{ij} E(\mathbf{x})) \delta(\partial_i E(\mathbf{x})),$$

where Heaviside function Θ_k is equal to 1 when the Hessian $\partial_{ij} E(\mathbf{x})$ has exactly k negative eigenvalues and 0 otherwise. Three aforementioned means are given by interrelated counting statistics:

- the total number of stationary points, $\mathcal{N}_{\text{eq}} = \sum_{k=0}^N \int \rho_k(\mathbf{x}) d\mathbf{x}$;
- the number of stationary points with instability index k , $\mathcal{N}_k = \int \rho_k(\mathbf{x}) d\mathbf{x}$;
- the number of stationary points with instability index up to k , $\mathcal{N}^{(k)} = \sum_{n=0}^k \int \rho_n(\mathbf{x}) d\mathbf{x}$.

Firstly, we combine density of stationary points $\rho_k(\mathbf{x})$ introduced in Eq. (13) with the multidimensional Kac-Rice formula:

$$\langle \mathcal{N}_k \rangle = \int d\mathbf{x} \left\langle |\det \partial_{ij} E(\mathbf{x})| \Theta_k(\partial_{ij} E(\mathbf{x})) \prod_{i=1}^N \delta(\partial_i E(\mathbf{x})) \right\rangle_V,$$

where $E(\mathbf{x})$ is the random function introduced in Eq. (1) and Heaviside function Θ_k outputs 1 when the Hessian has exactly k negative eigenvalues and 0 otherwise. Averaging is taken wrt. random field V .

Following [17], above average decouples since derived fields $\partial_i V$ and $\partial_{ij} V$ decouple as evidenced by vanishing of their cross-correlations $\langle \partial_i V \partial_{kl} V \rangle = 0$:

$$\left\langle |\det \partial_{ij} E(\mathbf{x})| \Theta_k(\partial_{ij} E(\mathbf{x})) \delta(\partial_i E(\mathbf{x})) \right\rangle_V = \left\langle |\det \partial_{ij} E(\mathbf{x})| \Theta_k(\partial_{ij} E(\mathbf{x})) \right\rangle_V \left\langle \delta(\partial_i E(\mathbf{x})) \right\rangle_V. \quad (14)$$

The first term is re-expressed using $\partial_{ij} E = \mu \delta_{ij} + \partial_{ij} V$ and by introducing an \mathbf{x} independent matrix M :

$$\left\langle |\det \partial_{ij} E(\mathbf{x})| \Theta_k(\partial_{ij} E(\mathbf{x})) \right\rangle_V = \left\langle |\det(\mu - M)| \Theta_k(\mu - M) \langle \delta(\partial V(\mathbf{x}) + M) \rangle_V \right\rangle_M. \quad (15)$$

where the average $\langle \delta(\partial V(\mathbf{x}) + M) \rangle_V$ is computed by first representing multidimensional delta function in terms of Fourier integral and then integrating out the V dependent term by using an identity $\langle [\text{Tr} P \partial V]^2 \rangle = \frac{\mu_c^2}{N} (2\text{Tr} P^2 + (\text{Tr} P)^2)$ with $\mu_c = \sqrt{f''(0)}$ defined previously. Due to Gaussianity of V , the integral does not depend on \mathbf{x} and is given by

$$\langle \delta(\partial V(\mathbf{x}) + M) \rangle_V \sim \exp\left(-\frac{N}{4\mu_c^2} \left(\text{Tr} M^2 - \frac{1}{3}(\text{Tr} M)^2\right)\right). \quad (16)$$

and is the random matrix joint pdf that we average over in formula (15). It is closely related to GOE since M is real and symmetric. Although the second term $\sim (\text{Tr} M)^2$ is non-standard, the formula can be recast into a proper GOE through introduction of an additional Gaussian integration and trivial rescaling. The result reads:

$$\left\langle |\det \partial_{ij} E(\mathbf{x})| \Theta_k(\partial_{ij} E(\mathbf{x})) \right\rangle_V = \sqrt{\frac{N}{2\pi}} \int_{-\infty}^{\infty} dt e^{-\frac{N}{2} t^2} \left\langle |\det(\mu + \mu_c t - M)| \Theta_k(\mu + \mu_c t - M) \right\rangle_{\text{GOE}}, \quad (17)$$

where the constant factor $\sqrt{\frac{N}{2\pi}}$ is specified in the $\mu \rightarrow \infty$ limit while average is taken over GOE with jpdf given by $P(M) = c_N^{-1} \exp\left(-\frac{N}{4\mu_c^2} \text{Tr} M^2\right)$ and $c_N = \mu_c^{N(N+1)/2} 2^{N/2} \left(\frac{2\pi}{N}\right)^{N(N+1)/4}$ is the normalization factor. Second term in (14) is computed trivially by Gaussian integration and reads:

$$\int d\mathbf{x} \left\langle \prod_{i=1}^N \delta(\partial_i E(\mathbf{x})) \right\rangle = \int \frac{d\mathbf{x}}{(i\sqrt{2\pi} f'(0))^N} \exp\left(\frac{\mu^2 \mathbf{x}^2}{2f'(0)}\right) = \frac{1}{\mu^N}. \quad (18)$$

Since the first term (17) is independent of \mathbf{x} , we integrate out the space-like variable \mathbf{x} as long as $f'(0) < 0$. Lastly, we bring together both terms (17) and (18) and find:

$$\langle \mathcal{N}_k \rangle = \frac{1}{\mu^N} \sqrt{\frac{N}{2\pi}} \int_{-\infty}^{\infty} dt e^{-\frac{N}{2} t^2} K_{k,N}(z_t), \quad (19)$$

where $z_t = \mu + \mu_c t$ and new notation for the matrix average is introduced:

$$K_{k,N}(z) = \langle |\det(z - M)| \Theta_k(z - M) \rangle_{\text{GOE}}, \quad (20)$$

Formula (19) is a generalization to $k \neq 0$ of equation found in [18]. Heaviside function is a symmetrized product each for eigenvalues of M :

$$\Theta_k(M) = \sum_{\sigma} \theta(-\lambda_{\sigma(1)}) \cdots \theta(-\lambda_{\sigma(k)}) \theta(\lambda_{\sigma(k+1)}) \cdots \theta(\lambda_{\sigma(N)}).$$

It conditions the matrix M to have exactly $N - k$ positive and k negative eigenvalues. To compute $K_{k,N}$ we follow the standard approach of random matrix theory [1] and change integration variables from matrix elements M_{ij} to its eigenvalues λ_i :

$$K_{k,N}(z) = z_N^{-1} \binom{N}{k} \int d\lambda_1 \cdots \int d\lambda_N \prod_{i < j} |\lambda_i - \lambda_j| \prod_{i=1}^N |z - \lambda_i| e^{-\frac{N}{4\mu_c^2} \lambda_i^2} \prod_{i=1}^k \theta(-z + \lambda_i) \prod_{i=k+1}^N \theta(z - \lambda_i). \quad (21)$$

The binomial is a combinatorial factor resulting from the symmetrization of Heaviside step function while $z_N = c_N 2^N \pi^{-\frac{N(N+1)}{4}} \prod_{i=1}^N \Gamma(1 + i/2) = (2\sqrt{2})^N \left(\frac{2\mu_c^2}{N}\right)^{N(N+1)/4} \prod_{j=1}^N \Gamma(1 + j/2)$ is the new normalization arising by integrating out the eigenvectors. In App. A we show how above quantity is proportional to the probability density of finding $(k + 1)$ -th largest eigenvalue:

$$K_{k,N}(z) = C_N e^{\frac{Nz^2}{4\mu_c^2}} \rho_{N+1}^{(k+1)}\left(z\sqrt{N/(2\mu_c^2)}\right), \quad (22)$$

where $\rho_{N+1}^{(k+1)}$ is probability density function of finding the $(k + 1)$ -th largest eigenvalue of a random matrix of size $(N + 1) \times (N + 1)$ and $C_N = \sqrt{2} \left(\frac{2}{N}\right)^{N/2} \mu_c^N \Gamma\left(\frac{N+1}{2}\right)$. We plug it back to Eq. (19) with rescaling $t \rightarrow \sqrt{2}t - m$ and obtain the final form given in Eq. (12):

$$\langle \mathcal{N}_k \rangle = c_N m^{-N} \sqrt{N} \int_{-\infty}^{\infty} ds e^{-Nf(s;m)} \rho_{N+1}^{(k+1)}\left(\sqrt{N}s\right), \quad (23)$$

where $\mu/\mu_c = m$, $c_N = \sqrt{\frac{2}{\pi}} \left(\frac{2}{N}\right)^{N/2} \Gamma\left(\frac{N+1}{2}\right)$ and $f(s;m) = \left(s - \frac{m}{\sqrt{2}}\right)^2 - \frac{s^2}{2}$. We readily calculate also formula for the cumulative variant $\langle \mathcal{N}^{(k)} \rangle$ as a sum:

$$\langle \mathcal{N}^{(k)} \rangle = c_N m^{-N} \sqrt{N} \int_{-\infty}^{\infty} ds e^{-Nf(s;m)} \sum_{n=0}^k \rho_{N+1}^{(n+1)}\left(\sqrt{N}s\right). \quad (24)$$

We stress that so far both formulas (23) and (24) are exact.

B. Calculating asymptotic forms of $\langle \mathcal{N}_k \rangle$ and $\langle \mathcal{N}^{(k)} \rangle$ across the transition

In this section we rederive asymptotics of Eqs. (23) and (24) in four regions detailed in Sec. IIB and Fig. 1. All results are summarized in Tab. I.

1. *Region a)* $m > 1, m \in O(1)$ and $k \in O(1)$

This case is straightforward as it has only one minimum and does not depend on m :

$$\langle \mathcal{N}_k(m) \rangle \sim \delta_{k,0}, \quad m > 1, \quad (25)$$

as was shown in [18] by the use of large deviation functions of probability density $\rho_{N+1}^{(k)}$.

2. *Region b)* $m = 1 + \delta/N^{1/3}$, $\delta > 0$ and $k \in O(1)$

We first calculate the asymptotics of prefactors and exponential factor in Eq. (23):

$$c_N(1 + \delta/N^{1/3})^{-N} e^{-Nf(s; 1 + \delta/N^{1/3})} \sim 2e^{-N(\frac{s^2}{2} - \sqrt{2}s + \frac{1}{2}) - 2\delta N^{2/3} + \sqrt{2}N^{2/3}\delta s - \delta^3/3} = 2e^{Ng(s; \delta)}. \quad (26)$$

We then calculate the integral (23) over s through saddle point method. To this end, we find the saddle from $g'(s; \delta) = 0$ as $s_* = \sqrt{2}$ and expand all terms around $s = s_* + \frac{1}{\sqrt{2}}\sigma N^{-2/3}$:

$$\langle \mathcal{N}_k(m = 1 + \delta N^{-1/3}) \rangle \sim 2e^{-\delta^3/3} \int_{-\infty}^{\infty} d\sigma e^{\delta\sigma} F'_k(\sigma), \quad \delta > 0, \quad (27)$$

where $\rho_{N+1}^{(k+1)}\left(\sqrt{2N} + \frac{\sigma}{\sqrt{2}N^{1/6}}\right) \sim \sqrt{2}N^{1/6}F'_k(\sigma)$ is the family of Tracy-Widom distributions [28, 29] for the $(k+1)$ -th largest eigenvalue of GOE. Cumulative mean (24) is given by a sum of $k+1$ contributions:

$$\langle \mathcal{N}^{(k)}(m = 1 + \delta/N^{1/3}) \rangle \sim 2e^{-\delta^3/3} \int_{-\infty}^{\infty} d\sigma e^{\delta\sigma} \sum_{n=0}^k F'_n(\sigma), \quad \delta > 0. \quad (28)$$

3. *Region c)* $m = 1 + \delta/N^{1/2}$, $\delta \in \mathbb{R}$ and $k = \kappa N^{1/4}$

In this region we use an approximate result found in [21, 26]. With $k = \kappa N^\gamma$ and for $\gamma \in (0, 1)$, the $(k+1)$ -th largest eigenvalue of GOE is asymptotically distributed as:

$$\rho_{N+1}^{(k+1)}(\sqrt{N}s) \sim \frac{1}{\sqrt{2\pi\sigma_k^2}} \exp\left(-\frac{(\sqrt{N}s - \mu_k)^2}{2\sigma_k^2}\right),$$

with mean $\mu_k = \sqrt{2N}\left(1 - \left(\frac{3\pi k}{4\sqrt{2N}}\right)^{2/3}\right)$ and variance $\sigma_k = \sqrt{\frac{2\log k}{\beta N^{1/3}(12\pi k)^{2/3}}}$. To calculate the cumulative mean (24) we first calculate the prefactor as:

$$c_N(1 + \delta N^{-1/2})^{-N} e^{-Nf(s; 1 + \delta N^{-1/2})} \sim 2e^{-N\left(\frac{s^2}{2} - \sqrt{2}s + \frac{1}{2}\right) - 2\delta\sqrt{N} + \sqrt{2N}\delta s} = 2e^{Ng(s; \delta)}. \quad (29)$$

From $g'(s; \delta) = 0$ we find the saddle-point at $s_* = \sqrt{2}$ and expand integrand around $s = s_* + \sigma/\sqrt{N}$:

$$Ng(s_* + \sigma/\sqrt{N}; \delta) \sim -\sigma^2/2 + \sqrt{2}\delta\sigma. \quad (30)$$

Now we turn to the asymptotic form of the sum inside the integral:

$$S_{\kappa N^\gamma}(\sqrt{N}s) = \sum_{k=0}^{\kappa N^\gamma} \rho_{N+1}^{(k)}(\sqrt{N}s)$$

in the general case $\gamma \in (0, 1)$. Since we inspect the $N \rightarrow \infty$ asymptotics, we approximate the sum as an integral by the Euler-Maclaurin formula:

$$S_{\kappa N^\gamma}(\sqrt{N}s) \sim N^\gamma \int_0^\kappa d\lambda \rho_{N+1}^{(\lambda N^\gamma)}(\sqrt{N}s) = D_N \int_0^\kappa d\lambda e^{\frac{N^{\frac{2}{3}}(2+\gamma)}{\log N} f(\lambda)} g(\lambda),$$

where $D_N = \sqrt{\frac{c_1}{\pi} \frac{N^{(1+8\gamma)/6}}{\sqrt{\log N}}}$, $f(\lambda; s) = -c_1 (s - \sqrt{2} + c_2 \lambda^{2/3} N^{2/3(\gamma-1)})^2 \lambda^{2/3}$ and $g(\lambda) = \lambda^{1/3}$ with constants $c_1 = \frac{1}{4\gamma} (12\pi)^{2/3}$ and $c_2 = \sqrt{2} \left(\frac{3\pi}{4\sqrt{2}} \right)^{2/3}$. In the next step we change variables $\lambda^{2/3} = x$, $\lambda^{1/3} d\lambda = \frac{3}{2} x dx$:

$$S_{\kappa N^\gamma}(\sqrt{N}s) \sim \frac{3}{2} D_N \int_0^{\kappa^{2/3}} x dx e^{\frac{N \frac{2}{3}(2+\gamma)}{\log N} \tilde{f}(x;s)},$$

where $\tilde{f}(x; s) = f(\lambda = x^{3/2}; s)$. Since we will eventually expand the sum around $s = s_* + \sigma/\sqrt{N}$, a natural scale is such that $\tilde{f}(x; \sqrt{2} + \sigma/N^{1/2}) = N^{-1} \tilde{f}_0(x; \sigma)$. This happens when $2/3(\gamma-1) = -1/2$ or the powers of N in both terms agree. From now on we set $\gamma = 1/4$:

$$S_{\kappa N^{1/4}}(\sqrt{N}s) \sim \frac{3}{2} D_N \int_0^{\kappa^{2/3}} x dx e^{\frac{\sqrt{N}}{\log N} \tilde{f}_0(x;\sigma)},$$

where $\tilde{f}_0(x; \sigma) = -c_1 (\sigma + c_2 x)^2 x$. Saddle point in above integral is given by $x_* = -\frac{\sigma}{c_2}$ and it must lie within the integration interval $x_* \in (0, \kappa^{2/3})$ otherwise its leading order contribution vanishes. We set $x = x_* + y \left(\frac{\sqrt{N}}{\log N} \right)^{-1/2}$ and compute the resulting integral:

$$S_{\kappa N^{1/4}}(\sqrt{N}s) \sim \frac{3}{2} D_N e^{\frac{\sqrt{N}}{\log N} \tilde{f}_0(x_*;\sigma)} x_* \sqrt{\frac{2\pi}{-\tilde{f}_0''(x_*;\sigma)} \frac{\sqrt{\log N}}{N^{1/4}}} \theta(x_*) \theta(\kappa^{2/3} - x_*).$$

Since $\theta(x_*) = \theta(-\sigma)$, $\theta(\kappa^{2/3} - x_*) = \theta(\sigma + c_2 \kappa^{2/3})$, $\tilde{f}_0(x_*; \sigma) = 0$ and $\tilde{f}_0''(x_*; \sigma) = 2c_1 c_2 \sigma$. Finally we obtain

$$S_{\kappa N^{1/4}}(\sqrt{N}s) \sim 2^{3/4} N^{1/4} \frac{1}{\pi} \sqrt{-\sigma} \theta(-\sigma) \theta(\sigma + c_2 \kappa^{2/3}). \quad (31)$$

We combine Eqs. (30) and (31) and plug them back to Eq. (24) which result in the final formula given in Tab. I:

$$\left\langle \mathcal{N}(\kappa N^{1/4})(m = 1 + \delta/N^{1/2}) \right\rangle \sim 2N^{1/4} \frac{2^{3/4}}{\pi} \int_0^{c_2 \kappa^{2/3}} d\sigma \sqrt{\sigma} e^{-\frac{\sigma^2}{2} - \sqrt{2}\sigma\delta}, \quad (32)$$

where $c_2 = \sqrt{2} \left(\frac{3\pi}{4\sqrt{2}} \right)^{2/3}$. For completeness we also take its derivative:

$$\frac{d}{d\kappa} \left\langle \mathcal{N}(\kappa N^{1/4})(m = 1 + \delta/N^{1/2}) \right\rangle \sim 2N^{1/4} \frac{2^{3/4}}{\pi} \left(\frac{2}{3} c_2^{3/2} e^{-\frac{c_2^2}{2} \kappa^{4/3} - \frac{\sqrt{2}}{2} c_2 \delta \kappa^{2/3}} \right). \quad (33)$$

4. Region d) $0 < m < 1$, $m \in O(1)$ and $k = \kappa N$

Lastly we deal with complex region with an extensive index variable. In this case we use result found in [21, 26] valid for $k = \kappa N$:

$$\rho_{N+1}^{(k+1)}(\sqrt{N}s) \sim \frac{1}{\sqrt{2\pi\sigma_k^2}} \exp\left(-\frac{(\sqrt{N}s - \mu_k)^2}{2\sigma_k^2}\right),$$

with $\mu_k = q_k \sqrt{2N}$ and $\sigma_k = \sqrt{\frac{\log N}{2N(1-q_k^2)}}$. The quantile parameter $q_k = t^{-1}(k/N)$ is the inverse cdf of the semicircle law:

$$t(\lambda) = \frac{2}{\pi} \int_\lambda^1 \sqrt{1-x^2} dx = \frac{1}{\pi} \left(\arccos \lambda - \lambda \sqrt{1-\lambda^2} \right). \quad (34)$$

It is expressed in terms of an inverse incomplete beta function defined through $b_{a,b}(B_{a,b}(z)) = z$ and where $b_{a,b}(z) = \int_0^z u^{a-1} (1-u)^{b-1} du$ and $t^{-1}(x) = 2B_{\frac{3}{2}, \frac{3}{2}}(1-x) - 1$. We follow essentially the same steps as in region c), the sum in Eq. (24) is asymptotically given by:

$$S_{\kappa N}(\sqrt{N}s) \sim N \int_0^\kappa d\lambda \rho_{N+1}^{(N\lambda)}(\sqrt{N}s) \sim \frac{N}{\sqrt{\pi}} \sqrt{\frac{N}{\log N}} \int_0^\kappa d\lambda e^{\frac{N^2}{\log N} \tilde{f}(\lambda)} g(\lambda),$$

with rescaled quantile function $Q_\lambda = q_{\lambda N}$ we denote $\tilde{f}(\lambda) = -(s - Q_\lambda\sqrt{2})^2(1 - Q_\lambda^2)$ and $g(\lambda) = \sqrt{1 - Q_\lambda^2}$. We find an approximate value for the integral by saddle point method. First, there are three saddles:

$$\begin{aligned}\lambda_*^0 &= 1 - B_{\frac{3}{2}, \frac{3}{2}} \left(\frac{1}{4}(2 - \sqrt{2}s) \right), \\ \lambda_*^\pm &= 1 - B_{\frac{3}{2}, \frac{3}{2}} \left(\frac{1}{16}(8 + \sqrt{2}s \pm \sqrt{32 + 2s^2}) \right),\end{aligned}$$

where λ_*^0 is the extremum. Leading order asymptotics is found when $\lambda_*^0 \in (0, \kappa)$, otherwise the integral is subleading. We expand $\lambda = \lambda_*^0 + x \left(\frac{N}{\sqrt{\log N}} \right)^{-1}$ and, after integrating out the x variable, find

$$S_{\kappa N}(\sqrt{N}s) \sim \frac{N}{\sqrt{\pi}} \sqrt{\frac{N}{\log N}} \frac{\sqrt{\log N}}{N} \sqrt{\frac{2\pi}{-\tilde{f}''(\lambda_*^0)}} e^{\frac{N^2}{\log N} \tilde{f}(\lambda_*^0)} g(\lambda_*^0) \theta(\lambda_*^0) \theta(\kappa - \lambda_*^0).$$

We evaluate some of the terms given above:

$$\begin{aligned}\theta(\lambda_*^0) &= \theta(\sqrt{2} - s), \\ \theta(\kappa - \lambda_*^0) &= \theta(s - \sqrt{2}Q_\kappa), \\ \tilde{f}(\lambda_*^0) &= 0, \\ g(\lambda_*^0) &= \sqrt{1 - s^2/2}, \\ f''(\lambda_*^0) &= -\pi^2.\end{aligned}$$

We bring these factors together and the sum $S_{\kappa N}(\sqrt{N}s)$ is equal to

$$S_{\kappa N}(\sqrt{N}s) \sim \sqrt{N} \frac{1}{\pi} \sqrt{2 - s^2} \theta(\sqrt{2} - s) \theta(s - \sqrt{2}Q_\kappa) \quad (35)$$

which is a semicircle law truncated at $s = \sqrt{2}Q_\kappa$. We plug back above formula to Eq. (24):

$$\langle \mathcal{N}^{(\kappa N)}(m) \rangle = c_N m^{-N} N \int_{\sqrt{2}Q_\kappa}^{\sqrt{2}} ds e^{-Nf(s;m)} \frac{1}{\pi} \sqrt{2 - s^2}.$$

Lastly, the large N contribution to above integral is found as:

$$\int_{\sqrt{2}Q_\kappa}^{\sqrt{2}} ds e^{-Nf(s;m)} \frac{1}{\pi} \sqrt{2 - s^2} \sim \frac{2}{\sqrt{\pi N}} \sqrt{1 - m^2} e^{\frac{Nm^2}{2}} \theta(1 - m) \theta(m - Q_\kappa)$$

while the prefactor reads $c_N m^{-N} N \sim 2N e^{-N/2 - N \ln m}$. Together they form the final result given in Tab. I:

$$\langle \mathcal{N}^{(\kappa N)}(m) \rangle \sim 4\sqrt{N/\pi} \sqrt{1 - m^2} \theta(1 - m) \theta(m - Q_\kappa) e^{N\Sigma_{\text{eq}}(m)}, \quad m \in (0, 1), \quad (36)$$

where $\Sigma_{\text{eq}}(m) = \frac{1}{2}(m^2 - 1) - \ln m$. The related pdf is found by differentiation:

$$\frac{d}{d\kappa} \langle \mathcal{N}^{(\kappa N)}(m) \rangle = 4\sqrt{N/\pi} \sqrt{1 - m^2} \theta(1 - m) \delta(\kappa - t(m)) e^{N\Sigma_{\text{eq}}(m)}, \quad m \in (0, 1),$$

where we used $\frac{d}{d\kappa} \theta(m - Q_\kappa) = \delta(\kappa - t(m))$. Closely related formula was found by different approach in [9, 19].

C. Mean number of all stationary points $\langle \mathcal{N}_{\text{eq}} \rangle$

To obtain mean number of all stationary points we can either follow the same route as in the previous section when deriving the fixed index case or simply use the fact that it is a special case of the cumulative distribution (24). For $k = N$ we find $\mathcal{N}_{\text{eq}} = \mathcal{N}^{(N)}$ since the sum of pdf's of individual eigenvalues summed over all eigenvalues gives the total density $\sum_{k=0}^N \rho_{N+1}^{(k+1)} = \rho_{N+1}$:

$$\langle \mathcal{N}_{\text{eq}} \rangle = c_N m^{-N} \sqrt{N} \int_{-\infty}^{\infty} ds e^{-Nf(s;m)} \rho_{N+1}(\sqrt{N}s). \quad (37)$$

D. Calculating asymptotic forms of $\langle \mathcal{N}_{\text{eq}} \rangle$ across the transition

In this section we compute asymptotics of Eqs. (37) in four regions detailed in Sec. IIB and Fig. 1. Due to similarities between Eq. (37) and Eqs. (23), (24) many steps in most derivations of asymptotic results we will use some formulas obtained in Sec. IIIB.

1. Region b) $m = 1 + \delta/N^{1/3}$, $\delta > 0$

Calculation of $\langle \mathcal{N}_{\text{eq}} \rangle$ in this region was found in [16]. The prefactor in this parameter region was already found in Eq. (26). Likewise, saddle point method applied to the integral produces the same formula (27). The only difference is in the integrand which we find in Prop. 9 of [14]:

$$\rho_N \left(y = \sqrt{2N} + \frac{\alpha}{\sqrt{2N^{1/6}}} \right) \sim \sqrt{2N^{1/6}} \rho_{\text{edge}}(\alpha), \quad (38)$$

where $\rho_{\text{edge}}(\alpha) = (\text{Ai}'(\alpha))^2 - \alpha(\text{Ai}(\alpha))^2 + \frac{1}{2}\text{Ai}(\alpha) \left(1 - \int_{\alpha}^{\infty} \text{Ai}(t) dt \right)$ is the microscopic spectral density of GOE near the edge. Final formula given in Tab. I reads:

$$\left\langle \mathcal{N}_{\text{eq}}(m = 1 + \delta N^{-1/3}) \right\rangle \sim 2e^{-\delta^3/3} \int_{-\infty}^{\infty} e^{\alpha\delta} \rho_{\text{edge}}(\alpha) d\alpha, \quad \delta > 0. \quad (39)$$

2. Region c) $m = 1 + \delta/N^{1/2}$, $\delta \in \mathbb{R}$

In this region the prefactor was already found in Eq. (26) and also the exponential term in Eq. (30). As in Sec. IIIB3, the integral over s is found through saddle point method around $s = \sqrt{2} + \sigma/N^{1/2}$ and the integrand reads:

$$\sqrt{N} ds \rho_{N+1}(\sqrt{N}s) = d\sigma \rho_{N+1}(\sqrt{2N} + \sigma) \sim d\sigma N^{1/4} \frac{2^{3/4}}{\pi} \sqrt{-\sigma} \theta(-\sigma),$$

where we used the macroscopic GOE spectral density $\rho_N(x) \sim \pi^{-1} \sqrt{2N - x^2}$. Lastly we collect these coefficients and so the final formula given in Tab. I reads:

$$\left\langle \mathcal{N}_{\text{eq}}(1 + \delta N^{-1/2}) \right\rangle \sim 2N^{1/4} \frac{2^{3/4}}{\pi} \int_0^{\infty} \sqrt{\sigma} e^{-\sigma^2/2 - \sqrt{2}\delta\sigma} d\sigma, \quad (40)$$

which, after rescaling $\sigma \rightarrow |\delta|\sigma$, recreates Eq. (102) of [16].

3. Region d) $0 < m < 1$, $m \in O(1)$

Finally we find mean number of all stationary points in the global region of complexity. Firstly we evaluate the integral of Eq. (37):

$$\int_{-\infty}^{\infty} ds e^{-Nf(s;m)} \rho_{N+1}(\sqrt{N}s)$$

using saddle point method. Solution to $f'(s;m) = 0$ gives the saddle $s_* = \sqrt{2m}$ and the integral is expanded around $s = s_* + \sigma N^{-1/2}$. Formula $-Nf(s_* + \sigma N^{-1/2}; m) = \frac{N}{2}m^2 - \sigma^2/2$ results in:

$$\int_{-\infty}^{\infty} ds e^{-Nf(s;m)} \rho_{N+1}(\sqrt{N}s) = \frac{e^{Nm^2/2}}{\sqrt{N}} \int_{-\infty}^{\infty} d\sigma e^{-\frac{1}{2}\sigma^2} \rho_{N+1}(\sqrt{2N}m + \sigma). \quad (41)$$

Spectral density ρ_N is again approximated using the semicircle law whose leading order behaviour reads:

$$\rho_N(\sqrt{2N}m + \sigma) \sim \frac{\sqrt{2N}}{\pi} \sqrt{1 - m^2}. \quad (42)$$

Above formula does not depend on σ so in Eq. (41) we are left with Gaussian integral $\int_{-\infty}^{\infty} d\sigma e^{-\frac{1}{2}\sigma^2} = \sqrt{2\pi}$. Asymptotic formula for the prefactor of $\langle \mathcal{N}_{\text{eq}} \rangle$ reads:

$$c_N m^{-N} \sqrt{N} \sim 2\sqrt{N} e^{-N/2 - N \ln m}, \quad (43)$$

Finally we collect Eqs. (41), (42) and (43) and the final result given in Tab. I is:

$$\langle \mathcal{N}_{\text{eq}}(m) \rangle \sim 4\sqrt{N/\pi} \sqrt{1-m^2} e^{N\Sigma_{\text{eq}}(m)}, \quad m \in (0, 1), \quad (44)$$

where $\Sigma_{\text{eq}}(m) = \frac{1}{2}(m^2 - 1) - \ln m$. Exponential part of this formula was calculated in Eq. (18) of [17].

Appendix A: Derivation of Eq. (22)

We establish relation (22):

$$K_{k,N}(z) = C_N e^{\frac{Nz^2}{4\mu_c^2}} \rho_{N+1}^{(k+1)} \left(z\sqrt{N/(2\mu_c^2)} \right),$$

where $C_N = \sqrt{2} \left(\frac{2}{N}\right)^{N/2} \mu_c^N \Gamma\left(\frac{N+1}{2}\right)$. We start off from l.h.s. given by Eq. (21):

$$K_{k,N}(z) = z_N^{-1} \binom{N}{k} \int d\lambda_1 \cdots \int d\lambda_N \prod_{i<j} |\lambda_i - \lambda_j| \prod_{i=1}^N |z - \lambda_i| e^{-\frac{N}{4\mu_c^2} \lambda_i^2} \prod_{i=1}^k \theta(-z + \lambda_i) \prod_{i=k+1}^N \theta(z - \lambda_i),$$

where $z_N = (2\sqrt{2})^N \left(\frac{2\mu_c^2}{N}\right)^{N(N+1)/4} \prod_{j=1}^N \Gamma(1+j/2)$. We integrate out the Heaviside functions, rescale $\lambda_i = \sqrt{\frac{2\mu_c^2}{N}} \mu_i$ and set $z = y\sqrt{\frac{2\mu_c^2}{N}}$ to find:

$$K_{k,N}(z) = z_N^{-1} \left(\frac{2\mu_c^2}{N}\right)^{N(N-1)/4+N} \tilde{\kappa}_{k,N}(y), \quad (A1)$$

with the rescaled quantity given by:

$$\tilde{\kappa}_{k,N}(y) = (-1)^k \binom{N}{k} \int_y^\infty d\mu_1 \cdots \int_y^\infty d\mu_k \int_{-\infty}^y d\mu_{k+1} \cdots \int_{-\infty}^y d\mu_N \prod_{i<j} |\mu_i - \mu_j| \prod_{i=1}^N (y - \mu_i) e^{-\frac{\mu_i^2}{2}}.$$

This quantity is related to the probability that exactly k eigenvalues lie inside an interval $J = (y, +\infty)$ (Def. 8.1 in [13]):

$$E_N(k, J) = \frac{1}{Z_{0,N}(-\infty)} \binom{N}{k} \int_y^\infty d\mu_1 \cdots \int_y^\infty d\mu_k \int_{-\infty}^y d\mu_{k+1} \cdots \int_{-\infty}^y d\mu_N \prod_{i<j} |\mu_i - \mu_j| e^{-\frac{\mu_i^2}{2}} = \frac{Z_{k,N}(y)}{Z_{0,N}(-\infty)}, \quad (A2)$$

where $Z_{0,N}(-\infty) = z_N \left(\mu_c = \sqrt{N/2}\right) = (2\sqrt{2})^N \prod_{j=1}^N \Gamma(1+j/2)$. Taking a derivative of E_N gives the pdf of the k -th largest eigenvalue $\rho_N^{(k)}$:

$$\begin{aligned} \frac{d}{dy} E_N(k, J) &= \rho_N^{(k+1)}(y) - \rho_N^{(k)}(y), \quad 1 \leq k \leq N-1, \\ \frac{d}{dy} E_N(0, J) &= \rho_N^{(1)}(y), \\ \frac{d}{dy} E_N(N, J) &= -\rho_N^{(N)}(y). \end{aligned}$$

In particular, setting $k=0$ gives the pdf of the largest eigenvalue. These formulas are found by using (A2) as a probability distribution. We sum first $k+1$ terms to obtain density $\rho_N^{(k)}$:

$$\frac{d}{dy} \left[\sum_{l=0}^k E_N(l, J) \right] = \rho_N^{(k)}(y). \quad (A3)$$

On the other hand, single derivative is related to the quantities $\tilde{\kappa}_{k,N}$ through:

$$\frac{d}{dy} E_{N+1}(k, J) = \frac{N+1}{Z_{0,N+1}(-\infty)} e^{-y^2/2} [\tilde{\kappa}_{k,N}(y) - \tilde{\kappa}_{k-1,N}(y)], \quad 1 \leq k \leq N,$$

along with $\frac{d}{dy} E_{N+1}(0, J) = \frac{N+1}{Z_{0,N+1}(-\infty)} e^{-y^2/2} \tilde{\kappa}_{0,N}(y)$. Due to telescopic property of the derivative, we sum up $k+1$ terms in order to find a formula for single $\tilde{\kappa}_{k,N}$:

$$\frac{d}{dy} \left[\sum_{l=0}^k E_{N+1}(l, J) \right] = \frac{N+1}{Z_{0,N+1}(-\infty)} e^{-y^2/2} \tilde{\kappa}_{k,N}(y). \quad (\text{A4})$$

We combine Eqs. (A1), (A3) and (A4) and plug back $y = z \sqrt{\frac{N}{2\mu_c^2}}$ to arrive at formula (22):

$$K_{k,N}(z) = C_N e^{\frac{Nz^2}{4\mu_c^2}} \rho_{N+1}^{(k+1)} \left(z \sqrt{N/(2\mu_c^2)} \right),$$

where constant prefactor is given by $C_N = z_N^{-1} \left(\frac{2\mu_c^2}{N} \right)^{N(N-1)/4+N} \frac{Z_{0,N+1}(-\infty)}{N+1} = \sqrt{2} \left(\frac{2}{N} \right)^{N/2} \mu_c^N \Gamma \left(\frac{N+1}{2} \right)$.

Appendix B: Model (1) with constraint $E_0 = E(\mathbf{x})$

In this section we consider a variant of the to model (1):

$$E(\mathbf{x}) = \frac{\mu}{2} \mathbf{x}^2 + V(\mathbf{x}), \quad \text{with } E_0 = E(\mathbf{x}), \quad (\text{B1})$$

where we restrict to solutions of fixed energy. In particular, we introduce means $\langle n_k \rangle$, $\langle n_{\text{eq}} \rangle$ and $\langle n^{(k)} \rangle$ analogous to quantities introduced in Sec. II A but with an additional term $\delta(E_0 - E(\mathbf{x}))$. Since both $\langle n_{\text{eq}} \rangle$ and $\langle n^{(k)} \rangle$ are easily derived from the cumulative mean $\langle n_k \rangle$, in what follows we consider only the latter quantity. Firstly, we write down its definition:

$$\langle n_k(E_0) \rangle = \int d\mathbf{x} \langle \rho_k(\mathbf{x}) \delta(E_0 - E(\mathbf{x})) \rangle_V, \quad (\text{B2})$$

where the E_0 dependence is explicitly stated. In accordance with previous comments, the mean number of stationary points with index k $\langle \mathcal{N}_k \rangle$ is related to formula (B2) through an integral $\langle \mathcal{N}_k \rangle = \int dE_0 \langle n_k(E_0) \rangle$. By essentially the same steps as in Sec. III A (also [19]), we arrive at the formula:

$$\langle n_k(E_0 = N\sqrt{f_0}\epsilon_0) \rangle = c_N m^{-N} \sqrt{N} \int_{-\infty}^{\infty} ds e^{-Nf(s;m)} G_N(s; m, \epsilon_0) \rho_{N+1}^{(k+1)}(s\sqrt{N}), \quad (\text{B3})$$

where function $f(s; m) = \left(s - \frac{m}{\sqrt{2}} \right)^2 - s^2/2$ and constant $c_N = \sqrt{\frac{2}{\pi}} \left(\frac{2}{N} \right)^{N/2} \Gamma \left(\frac{N+1}{2} \right)$. Geometric function G_N reads:

$$G_N(s; m, \epsilon_0) = g_N \int_0^{\infty} dR \frac{1}{R} e^{-Ng(R;m) - Nh(s,R;m,\epsilon_0)},$$

with constant $g_N = \sqrt{\frac{2}{\pi f_0 N}} \frac{q}{\sqrt{q^2-1}} \left(\frac{Nm^2}{2} \right)^{N/2} \frac{1}{\Gamma(N/2)}$, functions $g(R; m) = \frac{m^2}{2} R^2 - \ln R$ and $h(s, R; m, \epsilon_0) = \frac{1}{2(q^2-1)} \left[\sqrt{2}s - m + q\epsilon_0 - \frac{m}{2} R^2 \right]^2$.

We define parameters $m = \mu/\mu_c$ and $q = \mu_c/\tilde{\mu}_c$ with $\mu_c = \sqrt{f_0'}$, $\tilde{\mu}_c = -\frac{f_0'}{\sqrt{f_0}}$ and f is the correlation function defining the random field $V(\mathbf{x})$ with $f_0^{(k)} = f^{(k)}(0)$.

The formula for cumulative mean $\langle n_k \rangle$ given by (B3) is in a form resembling as the corresponding overall quantity $\langle \mathcal{N}_k \rangle$ given by Eq. (12) as closely as possible. The only additional factor is the geometric function G_N as the only term when the energy ϵ_0 enters into the formula. We can check that indeed $\int dE_0 G_N = 1$ and Eq. (B3) is reduced to previously studied Eq. (12). Also, we reduce to Eq. (12) in the limit $q \rightarrow \infty$ where $G_N \rightarrow 1$.

Lastly, we readily find an expression for the number of all stationary points at fixed energy E_0 as

$$\langle n_{\text{eq}}(E_0 = N\sqrt{f_0}\epsilon_0) \rangle = c_N m^{-N} \sqrt{N} \int_{-\infty}^{\infty} ds e^{-Nf(s;m)} G_N(s; m, \epsilon_0) \rho_{N+1}(s\sqrt{N}).$$

1. Phase space and calculating total mean $\langle n_{\text{eq}} \rangle$

We turn to inspecting phase space of this model which, in contrast to model (1), is now two-dimensional as we vary both coupling strength m and energy level ϵ_0 . In this section we first study only the behaviour of $\langle n_{\text{eq}}(E_0 = N\sqrt{f_0}\epsilon_0) \rangle$. Since the prefactor $c_N m^{-N} \sqrt{N} g_N \sim \sqrt{N}$, in what follows we calculate only the integral

$$I(m, \epsilon_0) = \int_{-\infty}^{\infty} ds \int_0^{\infty} dR \frac{1}{R} e^{-NF(s, R; m, \epsilon_0)} \rho_{N+1}(s\sqrt{N}), \quad (\text{B4})$$

with $F(s, R; m, \epsilon_0) = f(s; m) + g(R; m) + h(s, R; m, \epsilon_0)$. We first inspect the macroscopic phase space based on analysis of (B4). Resulting phase space is plotted in Fig. 2.

a. Macroscopic scale $m \in O(1)$ and $m < m_c$

We calculate leading order contribution via saddle-point method. We find relevant saddle points by $\partial_s F = 0, \partial_R F = 0$ as:

$$s_{\text{sp}} = \frac{\Delta(m, \epsilon_0) + q(mq - \epsilon_0)}{\sqrt{2}(1 + q^2)}, \quad R_{\text{sp}} = \frac{\sqrt{\Delta(m, \epsilon_0) - q(mq - \epsilon_0)}}{\sqrt{m}}, \quad (\text{B5})$$

where $\Delta(m, \epsilon_0) = \sqrt{2(1 + q^2) + q^2(mq - \epsilon_0)^2}$. Saddles were chosen so that both $R_{\text{sp}} > 0$ and $s_{\text{sp}} > 0$. The latter condition $s_{\text{sp}} > 0$ is true for values of $m \in (0, m_c)$ with

$$m_c = 1 + \frac{1 + 2q\epsilon_0}{2q^2}. \quad (\text{B6})$$

Equation $m = m_c$ in a picture of phase space is plotted in Fig. 2 as a dotted straight line. We expand the integral $I(m, \epsilon_0)$ around $s = s_{\text{sp}} + \sigma/N^{1/2}, R = R_{\text{sp}} + \rho/N^{1/2}$:

$$I(m, \epsilon_0) \sim \frac{1}{\sqrt{N}} e^{-NF_{\text{sp}}},$$

where $F_{\text{sp}} = F(s_{\text{sp}}, R_{\text{sp}})$ and we skipped the N -independent prefactor to focus on the complexity function:

$$\langle n_{\text{eq}}(E_0 = N\sqrt{f_0}\epsilon_0) \rangle \sim \sqrt{N} e^{N\Sigma_{\text{eq}}^{\leq}(m; \epsilon_0)}, \quad m < m_c, \quad (\text{B7})$$

with complexity function given by $\Sigma_{\text{eq}}^{\leq}(m, \epsilon_0) = -F(s_{\text{sp}}, R_{\text{sp}})$ with function F defined in Eq. (B4). Since $m > 0$ is positive, when m_c becomes negative, the leading contribution to $\langle n_{\text{eq}} \rangle$ vanishes. From $m_c = 0$ we find an energy threshold $(\epsilon_0)_{\text{th}} = -\frac{1+2q^2}{2q}$ below which complexity function is always negative (gray dot in the left plot of Fig. 2).

An implicit equation $F_{\text{sp}} = F(s_{\text{sp}}(m, \epsilon_0), R_{\text{sp}}(m, \epsilon_0)) = 0$ defines a curve in the (ϵ_0, m) plane (black thick line in Fig. 2) where the complexity function changes sign or when we move between simple and complex regions. Each point on that curve is denoted by $((\epsilon_0)_*, m_*)$. In particular, for value $(\epsilon_0)_{*, \text{max}} = -\frac{1}{2q}$ (dashed black line in Fig. 2) sign change happens at $m_{*, \text{max}} = 1$.

For $\epsilon_0 = (\epsilon_0)_{*, \text{max}}$ and in the large q limit, we recreate complexity function in the complex region given by Eq. (44) as $\lim_{q \rightarrow \infty} \Sigma_{\text{eq}}^{\leq}(m, \epsilon_0 = -\frac{1}{2q}) = \frac{m^2 - 1}{2} - \log m = \Sigma_{\text{eq}}$.

b. Macroscopic scale $m \in O(1)$ and $m > m_c$

In the $m > m_c$ with m_c defined in Eq. (B6), we use large deviation results for the spectral density:

$$\rho_{N+1}(s\sqrt{N}) \sim e^{-N\phi(s)}, \quad \phi(s) = \frac{1}{2}s\sqrt{s^2 - 2} - \ln\left(\frac{s + \sqrt{s^2 - 2}}{\sqrt{2}}\right), \quad s > \sqrt{2},$$

and compute the resulting integral $I(m, \epsilon_0)$:

$$I(m, \epsilon_0) \sim \int_{\sqrt{2}}^{\infty} \int_{-\infty}^{\infty} \frac{dR}{R} ds e^{-N\mathcal{F}}, \quad \mathcal{F} = F + \phi,$$

where F was defined before in the $m < m_c$ case in Eq. (B4). From now on we track only the exponential part. From $\partial_s \mathcal{F} = 0, \partial_R \mathcal{F} = 0$ we find saddles as

$$s'_{\text{sp}} = \frac{1}{2\sqrt{2}q} \left((mq - \epsilon_0)(1 + 2q^2) + (1 - 2q^2)\sqrt{(mq - \epsilon_0)^2 - 2} \right),$$

$$R'_{\text{sp}} = \sqrt{\frac{q}{m}} \sqrt{mq - \epsilon_0 - \sqrt{(mq - \epsilon_0)^2 - 2}},$$

where from $s'_{\text{sp}} > \sqrt{2}$ we read off the condition $m > m_c$ with m_c given by Eq. (B6). The exponential contribution to the integral is $I(m, \epsilon_0) \sim e^{-N\mathcal{F}_{\text{sp}}}$ with $\mathcal{F}_{\text{sp}} = F(s'_{\text{sp}}, R'_{\text{sp}}) + \phi(s'_{\text{sp}})$. The mean total number is given by

$$\left\langle n_{\text{eq}}(E_0 = N\sqrt{f_0}\epsilon_0) \right\rangle \sim e^{N\Sigma_{\text{eq}}^{\geq}(m; \epsilon_0)}, \quad m > m_c, \quad (\text{B8})$$

where $\Sigma_{\text{eq}}^{\geq}(m; \epsilon_0) = -F(s'_{\text{sp}}, R'_{\text{sp}}) - \phi(s'_{\text{sp}})$. Function $\mathcal{F}_{\text{sp}} = 0$ vanishes for $\epsilon_0 = -\frac{1}{2q}$ and $m > m_c$. For different values of ϵ_0 we find $\mathcal{F}_{\text{sp}} > 0$ and so the complexity function is negative.

In the left plot of Fig. 2 we sketch the resulting macroscopic phase space. We identify two boundaries where the behaviour of complexity function changes – where the function changes between positive and negative given implicitly by $F_{\text{sp}} = 0$ (thick solid line in Fig. 2) and where the complexity function changes its functional form when $m = m_c$ (slanted dotted line in Fig. 2). In the unconstrained model (1) both boundaries coincide and the transition region is easily defined. In this case we extend the definition and mark the transition region when both $m = m_c$ and $F_{\text{sp}} = 0$. From the left plot in Fig. 2 we identify two points on the phase space when these conditions are met – $(0, (\epsilon_0)_{\text{th}})$ and $(m_{*,\text{max}}, (\epsilon_0)_{*,\text{max}})$. Only the latter point is nontrivial and we continue to investigate the model on a microscopic scale around this critical point.

c. Microscopic scale in the vicinity of $(m_{*,\text{max}}, (\epsilon_0)_{*,\text{max}})$

We expand complexity functions at the boundary $m = m_c$:

$$\Sigma_{\text{eq}}^{\leq}(m) \sim \Sigma_{\text{eq}}^{\leq}(m_c) + (m - m_c)\Sigma_{\text{eq}}^{\leq}(m_c)' + \frac{1}{2}(m - m_c)^2\Sigma_{\text{eq}}^{\leq}(m_c)'' + \dots,$$

$$\Sigma_{\text{eq}}^{\geq}(m) \sim \Sigma_{\text{eq}}^{\geq}(m_c) + (m - m_c)\Sigma_{\text{eq}}^{\geq}(m_c)' + \frac{1}{2}(m - m_c)^2\Sigma_{\text{eq}}^{\geq}(m_c)'' + \dots,$$

where from explicit formulas for both complexity functions we find two first terms in the expansion equal $\Sigma_{\text{eq}}^{\leq}(m_c) = \Sigma_{\text{eq}}^{\geq}(m_c)$, $\Sigma_{\text{eq}}^{\leq}(m_c)' = \Sigma_{\text{eq}}^{\geq}(m_c)'$ and the discontinuity happens for the third term $\Sigma_{\text{eq}}^{\leq}(m_c)'' \neq \Sigma_{\text{eq}}^{\geq}(m_c)''$. Hence, the proper microscopic scaling is

$$m = m_c + \delta/N^{1/2}, \quad \epsilon_0 = (\epsilon_0)_c + \epsilon/N^{1/2}$$

with points related by $m_c = 1 + \frac{1+2q(\epsilon_0)_c}{2q^2}$. It contains the critical point $(m, \epsilon_0) = (m_{*,\text{max}}, (\epsilon_0)_{*,\text{max}}) = \left(1, -\frac{1}{2q}\right)$ which we deal with in what follows. In the right plot of Fig. 2 we graph a detailed picture of phase space near this critical point.

By standard saddle point analysis we expand the integral (B4) around $(m_{*,\text{max}}, (\epsilon_0)_{*,\text{max}})$ as:

$$I \left(m = 1 + \delta/N^{1/2}, \epsilon_0 = -\frac{1}{2q} + \epsilon/N^{1/2} \right) \sim \frac{c'_N}{N} \int_{-\infty}^{\infty} d\sigma e^{\frac{2\sqrt{2}q(q\delta - \epsilon)}{2q^2 - 1}\sigma - \frac{2q^2 + 3}{2(2q^2 - 1)}\sigma^2} \rho_{N+1}(\sqrt{2N} + \sigma).$$

with constant $c'_N = \sqrt{2\pi} \sqrt{\frac{q^2 - 1}{2q^2 - 1}} e^{-\frac{(\delta - 2q\epsilon)^2}{4(2q^2 - 1)}}$. We use the semicircle law $\rho_{N+1}(\sqrt{2N} + \sigma) \sim N^{1/4} \frac{2^{3/4}}{\pi} \sqrt{-\sigma\theta(-\sigma)}$ and obtain the mean number of minima with energy $\epsilon_0 = (\epsilon_0)_{*,\text{max}} + \epsilon/N^{1/2}$:

$$\left\langle n_{\text{eq}}(m = m_{*,\text{max}} + \delta/N^{1/2}; E_0 = N\sqrt{f_0}(\epsilon_0)_{*,\text{max}} + \sqrt{Nf_0}\epsilon) \right\rangle \sim N^{1/4} \int_0^{\infty} d\sigma \sqrt{\sigma} e^{-\frac{\sigma^2}{2} - \frac{a_1}{\sqrt{2a_2}}\sigma}, \quad (\text{B9})$$

where $a_1 = \frac{2\sqrt{2}q(q\delta - \epsilon)}{2q^2 - 1}$, $a_2 = \frac{2q^2 + 3}{2(2q^2 - 1)}$ and an unspecified prefactor.

d. *Microscopic scale in the vicinity of $m = m_c$*

In the previous section we investigated the vicinity of one point in the phase space marked by gray square in both plots of Fig. 2. Now we look at behaviour around $m = m_c$ (a dotted black line in Fig. 2). $m = m_c + \delta/N^{1/2}$, $\epsilon_0 = (\epsilon_0)_c + \epsilon/N^{1/2}$. The result reads

$$\left\langle n_{\text{eq}} \left(m = m_c + \delta/N^{1/2}; E_0 = N\sqrt{f_0}((\epsilon_0)_c + \epsilon/N^{1/2}) \right) \right\rangle \sim e^{N\Delta_0 + \sqrt{N}\Delta_1 + \Delta_2} \int_0^\infty d\sigma \sqrt{\sigma} e^{-\frac{\sigma^2}{2} - \frac{a_1}{\sqrt{2a_2}}\sigma},$$

with $\Delta_0 = -\frac{1}{2} \log m_c - \frac{1}{2}(1 - m_c)(1 + q^2(1 - m_c))$, $\Delta_1 = \frac{1 - m_c}{2m_c}(2qm_c\epsilon - \delta)$, $\Delta_2 = \frac{4qm_c^2\epsilon(\delta - \epsilon q) - \delta^2(2q^2(m_c^2 - 1) + 1)}{4m_c^2(2q^2 - 1)}$ and a_1, a_2 defined before. For all values of m besides the critical value $m = m_{*,\text{max}} = 1$, the exponent function $\Delta_0 < 0$ is negative so the overall mean number of stationary points $\langle n_{\text{eq}} \rangle$ is exponentially small in N . Hence, along the line $m = m_c$ besides $m = 1$ the fractional probabilities (5) lose its interpretation when the counting function in the denominator is vanishing asymptotically with N .

2. Calculating cumulative means $\langle n^{(k)} \rangle$

We move to calculate the cumulative mean $\langle n^{(k)} \rangle$ being a sum of Eq. (B3):

$$\left\langle n^{(k)} \left(m; E_0 = N\sqrt{f_0}\epsilon_0 \right) \right\rangle = c_N m^{-N} \sqrt{N} g_N \int_{-\infty}^\infty ds \int_0^\infty \frac{dR}{R} e^{-NF(s,R;m,\epsilon_0)} S_k(s\sqrt{N}),$$

where $S_k(s\sqrt{N}) = \sum_{n=0}^k \rho_{N+1}^{(n+1)}(s\sqrt{N})$. We already asymptotically approximated these sums in two relevant cases with $k = \kappa N^{1/4}$ for Eq. (31) and $k = \kappa N$ in Eq. (35).

a. *Macroscopic scale $m < m_c$ and $k = \kappa N$*

We use the result of (35) $S_{\kappa N}(\sqrt{N}s) \sim \frac{\sqrt{N}}{\pi} \sqrt{2 - s^2} \theta(\sqrt{2} - s) \theta(s - \sqrt{2}Q_\kappa)$ where Q_κ is the quantile function defined as the inverse of semicircle law (34). We essentially follow the same steps as in Sec. III B 3 when asymptotics of $\mathcal{N}^{(k)}$ were conducted. We combine it with the same saddle point analysis as in derivation of $\langle n_{\text{eq}} \rangle$ asymptotics and arrive at:

$$\left\langle n^{(\kappa N)}(m; E_0 = N\sqrt{f_0}\epsilon_0) \right\rangle \sim \theta_{s_{\text{sp}} \in (\sqrt{2}Q_\kappa, \sqrt{2})} e^{N\Sigma_{\text{eq}}^{\leq}(m;\epsilon_0)}, \quad (\text{B10})$$

where the saddle point s_{sp} is given by Eq. (B5).

b. *Microscopic scale near $(m_{*,\text{max}}, (\epsilon_0)_{*,\text{max}})$ and $k = \kappa N^{1/4}$*

We use a derivation of $\langle n_{\text{eq}} \rangle$ but with the result Eq. (31) for $S_{\kappa N^{1/4}}(\sqrt{N}s) \sim 2^{3/4} N^{1/4} \frac{1}{\pi} \sqrt{-\sigma} \theta(-\sigma) \theta(\sigma + c_2 \kappa^{2/3})$. The formula reads

$$\left\langle n^{(\kappa N^{1/4})} \left(m = 1 + \delta/N^{1/2}; E_0 = -\frac{N\sqrt{f_0}}{2q} + \sqrt{Nf_0}\epsilon \right) \right\rangle \sim N^{1/4} \int_0^{\sqrt{2a_2 c_2 \kappa^{2/3}}} d\sigma \sqrt{\sigma} e^{-\frac{\sigma^2}{2} - \frac{a_1}{\sqrt{2a_2}}\sigma}, \quad (\text{B11})$$

where the notation is the same as in Eq. (B9).

3. Calculating probabilities P_k

We calculated both total $\langle n_{\text{eq}} \rangle$ and cumulative $\langle n^{(k)} \rangle$ means for $m < m_c$ and around $m = m_{*,\text{max}}$. These correspond to regions c) and d) introduced in the paper and describing toppling and complexity respectively. Since the aim of this Appendix is to present the toppling mechanism in the fixed energy model (B1), we altogether skip the simplicity and hierarchy regions a) and b).

a. *Region c)* $m = m_{*,\max} + \delta/N^{1/2}$, $\epsilon_0 = (\epsilon_0)_{*,\max} + \epsilon/N^{1/2}$ and $k = \kappa N^{1/4}$

We use the formulas (5) for annealed probabilities and simply calculate the ratio of Eqs. (B9) and (B11):

$$P_{\kappa N^{1/4}}(\delta, \epsilon; q) \sim \frac{\int_0^{C_2 \kappa^{2/3}} d\sigma \sqrt{\sigma} e^{-\frac{\sigma^2}{2} - \Delta\sigma}}{\int_0^\infty d\sigma \sqrt{\sigma} e^{-\frac{\sigma^2}{2} - \Delta\sigma}}$$

where the parameters read

$$C_2 = \sqrt{\frac{2q^2 + 3}{2q^2 - 1}} \sqrt{2} \left(\frac{3\pi}{4\sqrt{2}} \right)^{2/3}, \quad \Delta = \frac{2q^2(\delta - \epsilon/q)}{\sqrt{(2q^2 - 1)(q^2 + 2)}}. \quad (\text{B12})$$

Corresponding probability formula for the toy model (1) given in Tab. I has the same form with different parameters. An easy check ensures these parameters reduce in the large q limit $\lim_{q \rightarrow \infty} C_2 = c_2$ and $\lim_{q \rightarrow \infty} \Delta = \sqrt{2}\delta$. The tipping point for the toppling mechanism in this model is for $\Delta = 0$ or when $\delta = \epsilon/q$. The maximum instability index in this model reads $\kappa'_{\max} = \left(-\frac{\Delta}{C_2} \right)^{3/2} = \left(-\frac{2q^2(\delta - \epsilon/q)}{c_2 \sqrt{(2+q^2)(2q^2+3)}} \right)^{3/2}$. Therefore, the underlying mechanism has the same characteristics as in the toy model (1) shown in Fig. 1.

b. *Region d)* $m < m_c$

Ratio of (B7) and (B10) gives:

$$P_{\kappa N}(m, \epsilon_0; q) \sim \frac{\theta_{s_{\text{sp}} \in (\sqrt{2}Q_\kappa, \sqrt{2})}}{\theta_{s_{\text{sp}} \in (0, \sqrt{2})}}, \quad (\text{B13})$$

where $s_{\text{sp}} = \frac{\Delta(m, \epsilon_0) + q(mq - \epsilon_0)}{\sqrt{2(1+q^2)}}$ and $\Delta(m, \epsilon_0) = \sqrt{2(1+q^2) + q^2(mq - \epsilon_0)^2}$. We recast conditions on saddle point into that for m, ϵ and so $s_{\text{sp}} > 0$ means $m > 0$, $s_{\text{sp}} < \sqrt{2}$ is translated to $m < m_c$ while $s_{\text{sp}} > \sqrt{2}Q_\kappa$ means $m > m_+$ with m_+ known only implicitly. For $m \in (0, m_c)$, the denominator in (B13) is always equal to 1 and moreover we can invert the second inequality $\theta(s_{\text{sp}} > \sqrt{2}Q_\kappa) = \theta(\kappa - t(s_{\text{sp}}/\sqrt{2}))$ with cdf t given by Eq. (34):

$$t(s) = \frac{2}{\pi} \int_s^1 \sqrt{1-x^2} dx.$$

As a check, we study $q \rightarrow \infty$ limit where $\lim_{q \rightarrow \infty} s_{\text{sp}} = \sqrt{2}m$ which again reduces to the formula found in Tab. I. Finally, the cdf reads $P_{\kappa N}(m, \epsilon_0; q) \sim \theta(\kappa - t(s_{\text{sp}}/\sqrt{2}))$ while its pdf is a delta function:

$$\frac{d}{d\kappa} P_{\kappa N}(m, \epsilon_0; q) \sim \delta(\kappa - t(s_{\text{sp}}/\sqrt{2})).$$

Appendix C: Spherical spin-glass model

In this section we consider statistics of stationary points in a variant of spherical spin-glass model following closely [16]. The energy function we consider reads:

$$E_o(\mathbf{x}) = \sum_{i_1, \dots, i_p=1}^{N+1} J_{i_1, i_2, \dots, i_p} x_{i_1} x_{i_2} \dots x_{i_p} + \sum_{i=1}^{N+1} h_i x_i,$$

where \mathbf{x} is now an $N+1$ dimensional vector constrained to lie on the sphere $\sum_{i=1}^{N+1} x_i^2 = N$ and $p \geq 2$ is an integer. Symmetric coupling matrix J and random external field h_i are both drawn from a Gaussian distribution with mean and variance given by:

$$\begin{aligned} \langle J_{i_1, i_2, \dots, i_p} \rangle &= 0, & \langle (J_{i_1, i_2, \dots, i_p})^2 \rangle &= \frac{J^2}{pN^{p-1}}, \\ \langle h_i \rangle &= 0, & \langle h_i^2 \rangle &= \sigma^2. \end{aligned}$$

If we treat the energy itself as a random field, its covariance structure reads:

$$\begin{aligned}\langle E_o(\mathbf{x}) \rangle &= 0, \\ \langle E_o(\mathbf{x}) E_o(\mathbf{x}') \rangle &= N \tilde{f} \left(\frac{\mathbf{x} \cdot \mathbf{x}'}{N} \right),\end{aligned}$$

with correlation function $\tilde{f}(u) = \frac{J^2}{p} u^p + \sigma^2 u$. We follow [16] and arrive at a formula for the mean counting function:

$$\langle \mathcal{N}_k \rangle_o = \bar{c}_{J,p,\sigma} \sqrt{\frac{N}{2\pi}} \int dt e^{-\frac{N}{2} t^2} K'_{k,N}(z_t),$$

where $\bar{c}_{J,p,\sigma} = \frac{2\sqrt{\pi}}{\Gamma(\frac{N+1}{2})} \left(\frac{2}{N} (J^2 + \sigma^2) \right)^{-N/2}$ and $z_t = t \sqrt{J^2 p + \sigma^2}$. Average K' is given by

$$K'_{k,N}(z) = \langle |\det(z - H)| \Theta_k(z - H) \rangle_H,$$

where H is a GOE with jPDF $P(H) \sim \exp\left(-\frac{N}{4J^2(p-1)} \text{Tr} H^2\right)$. Lastly we use relation (22) with replacement $\mu_c^2 \rightarrow J^2(p-1)$ stemming from a different normalization of the random matrix and find:

$$K'_{k,N}(z) = C_N e^{\frac{Nz^2}{4J^2(p-1)}} \rho_{N+1}^{(k+1)} \left(\frac{z}{\sqrt{2J^2(1-p)}} \sqrt{N} \right),$$

with $C_N = \sqrt{2} \left(\frac{2J^2(p-1)}{N} \right)^{N/2} \Gamma\left(\frac{N+1}{2}\right)$. We plug it back, rescale $t = s \sqrt{\frac{2J^2(p-1)}{J^2 p + \sigma^2}}$ and find

$$\langle \mathcal{N}_k \rangle_o = c'_N \int ds e^{-\frac{N}{2} \frac{J^2(p-2) - \sigma^2}{J^2 p + \sigma^2} s^2} \rho_{N+1}^{(k+1)}(\sqrt{N}s),$$

with $c'_N = 2\sqrt{2N} \sqrt{\frac{J^2(p-1)}{J^2 p + \sigma^2}} \left(\frac{J^2(p-1)}{J^2 + \sigma^2} \right)^{N/2}$. Lastly we introduce a single parameter $B = \frac{J^2(p-2) - \sigma^2}{J^2 p + \sigma^2}$ so that

$$\langle \mathcal{N}_k \rangle_o = c'_N \int ds e^{-\frac{NB}{2} s^2} \rho_{N+1}^{(k+1)}(\sqrt{N}s), \quad (\text{C1})$$

where the constant reads $c'_N = 2\sqrt{N} \left(\frac{1+B}{1-B} \right)^{\frac{N+1}{2}} \sqrt{1-B}$. We observe that for $p \geq 2$, the parameter $B \in \left(-1, \frac{p-2}{p}\right]$. For completeness we also write down the total and the cumulative number of stationary points:

$$\begin{aligned}\langle \mathcal{N}^{(k)} \rangle_o &= c'_N \int ds e^{-\frac{NB}{2} s^2} \sum_{n=0}^k \rho_{N+1}^{(n+1)}(\sqrt{N}s), \\ \langle \mathcal{N}_{\text{eq}} \rangle_o &= c'_N \int ds e^{-\frac{NB}{2} s^2} \rho_{N+1}(\sqrt{N}s).\end{aligned}$$

Formula for $\langle \mathcal{N}_{\text{eq}} \rangle_o$ agrees with Eq. (41) of [16].

1. Regions

According to [16], there exist four regions of change as in the toy model (1). Parameter B combining J , σ and p serves a role analogous to the coupling strength m . Scales for B and also index variable k in all four regions are summarized in Tab. ???. As before, regions a) and d) are macroscopic with $B \in O(1)$ and region b), c) are microscopic with $B \in O(N^{-1/3})$ and $B \in O(N^{-1})$. Toppling region has a different scaling in comparison to the toy model (1) where m scaled as $O(N^{-1/2})$. Consequently, the instability index scaling is $k = \kappa N$ in both regions c) and d).

2. Results on the total mean number $\langle \mathcal{N}_{\text{eq}} \rangle_o$

$\langle \mathcal{N}_{\text{eq}} \rangle_o$ across all four regions of change was calculated in [16]. These results are summarized in the last column of Tab. II. In comparison to Tab. I, regions a) and b) look similar although due to topological constraints, minimal number of total stationary points is 2. Regions c) and d) behave similarly to analogous regions in the toy model although the scaling with N in c) is different.

3. Results on the cumulative mean number $\langle \mathcal{N}^{(k)} \rangle_{\circ}$

Although previously we mainly cited [16], in this section most formulas are completely or partially new. We expand cumulative means around points of total stability $k = 0$ and total instability $k = N$ due to topological constraints present in the system. In particular, this constraint is most clearly manifested in the total number of all stationary points $\langle \mathcal{N}_{\text{eq}} \rangle_{\circ}$ being equal to 2 in the simple region a). Closer inspection conducted in [16] reveals that stationary points in the simple region are necessarily a total minimum with instability index $k = 0$ and a total maximum with $k = N$. This fact has consequences also in the toppling region c).

4. Calculating probabilities P_k

With the knowledge of $\langle \mathcal{N}^{(k)} \rangle_{\circ}$ and $\langle \mathcal{N}_{\text{eq}} \rangle_{\circ}$ the annealed probabilities, Eq. (5), are easily computed from the results in the previous two sections. The results are summarized in Tab. II. Aforementioned topological constraint is manifested across all regions as symmetries of pdfs upon substitutions $k \rightarrow N - k$ and $\kappa \rightarrow 1 - \kappa$. All results in this section are presented in Fig. 3 where the symmetry is evident.

-
- [1] G. Akemann, J. Baik, and Ph. Di Francesco, editors. *The Oxford handbook of random matrix theory*. Oxford University Press, Oxford, 2011.
 - [2] A. Auffinger and G. Ben Arous. Complexity of random smooth functions on the high-dimensional sphere. *Ann Probab*, 41(6):4214–4247, 11 2013.
 - [3] A. Auffinger, G. Ben Arous, and J. Černý. Random matrices and complexity of spin glasses. *Commun Pure Appl Math*, 66(2):165–201, 2013.
 - [4] A. Auffinger and J. Gold. The number of saddles of the spherical p-spin model. *arXiv:2007.09269*, 2020.
 - [5] A.J. Ballard, R. Das, S. Martiniani, D. Mehta, L. Sagun, J.D. Stevenson, and D.J. Wales. Energy landscapes for machine learning. *Phys. Chem. Chem. Phys.*, 19:12585–12603, 2017.
 - [6] G. Ben Arous, A. Dembo, and A. Guionnet. Aging of spherical spin glasses. *Probability Theory and Related Fields*, 120(1):1–67, 2001.
 - [7] G. Ben Arous, Y. V. Fyodorov, and B. A. Khoruzhenko. Counting equilibria of large complex systems by instability index. *arXiv:2008.00690*, 2020.
 - [8] F. Bornemann. On the numerical evaluation of distributions in random matrix theory: a review. *Markov Process. Related Fields*, 16(4):803–866, 2010.
 - [9] A.J. Bray and D.S. Dean. Statistics of critical points of Gaussian fields on large-dimensional spaces. *Phys Rev Lett*, 98:150201, Apr 2007.
 - [10] A. Choromanska, M. Henaff, M. Mathieu, G. Ben Arous, and Y. Lecun. The loss surfaces of multilayer networks. *arXiv:1412.0233*, 2014.
 - [11] G. Christakos. *Spatiotemporal Random Fields, 2nd ed.* Elsevier, 2017.
 - [12] A. Crisanti and H. J. Sommers. The spherical-p-spin interaction spin glass model: the statics. *Zeitschrift für Physik B Condensed Matter*, 87(3):341–354, 1992.
 - [13] P. J. Forrester. *Log-gases and random matrices*, volume 34 of *London Mathematical Society Monographs Series*. Princeton University Press, Princeton, NJ, 2010.
 - [14] P. J. Forrester, N. E. Frankel, and T. M. Garoni. Asymptotic form of the density profile for Gaussian and Laguerre random matrix ensembles with orthogonal and symplectic symmetry. *J. Math. Phys.*, 47(2):023301, 26, 2006.
 - [15] S. Franz and M. Mézard. Off-equilibrium glassy dynamics: A simple case. *Europhysics Letters (EPL)*, 26(3):209–214, apr 1994.
 - [16] Y. V. Fyodorov. High-dimensional random fields and random matrix theory. *Markov Process. Related Fields*, 21(3, part 1):483–518, 2015.
 - [17] Y.V. Fyodorov. Complexity of random energy landscapes, glass transition, and absolute value of the spectral determinant of random matrices. *Phys Rev Lett*, 92:240601, Jun 2004.
 - [18] Y.V. Fyodorov and C. Nadal. Critical behavior of the number of minima of a random landscape at the glass transition point and the Tracy-Widom distribution. *Phys Rev Lett*, 109:167203, Oct 2012.
 - [19] Y.V. Fyodorov and I. Williams. Replica symmetry breaking condition exposed by random matrix calculation of landscape complexity. *J Stat Phys*, 129:1081–1116, 2007.
 - [20] I. Goodfellow, Y. Bengio, and A. Courville. *Deep Learning*. MIT Press, 2016. <http://www.deeplearningbook.org>.
 - [21] J. Gustavsson. Gaussian fluctuations of eigenvalues in the GUE. *Ann. Inst. H. Poincaré Probab. Statist.*, 41(2):151–178, 2005.
 - [22] J. M. Kosterlitz, D. J. Thouless, and R.C. Jones. Spherical model of a spin-glass. *Phys. Rev. Lett.*, 36:1217–1220, May 1976.

- [23] J. Kurchan and L. Laloux. Phase space geometry and slow dynamics. *J Phys A Math Gen*, 29(9):1929–1948, may 1996.
- [24] Y. LeCun, Y. Bengio, and G. Hinton. Deep learning. *Nature*, 521(7553):436–444, 2015.
- [25] A. Lucas. Ising formulations of many np problems. *Frontiers in Physics*, 2:5, 2014.
- [26] S. O’Rourke. Gaussian fluctuations of eigenvalues in Wigner random matrices. *J. Stat. Phys.*, 138(6):1045–1066, 2010.
- [27] E. Subag. The complexity of spherical p -spin model – a second moment approach. *Ann Probab*, 45(5):3385–3450, 09 2017.
- [28] C.A. Tracy and H. Widom. Level-spacing distributions and the Airy kernel. *Comm. Math. Phys.*, 159(1):151–174, 1994.
- [29] C.A. Tracy and H. Widom. Fredholm determinants and the mKdV/sinh-Gordon hierarchies. *Comm. Math. Phys.*, 179(1):1–9, 1996.
- [30] D.J. Wales. *Energy Landscapes: Applications to Clusters, Biomolecules and Glasses*. Cambridge University Press, 2004.